Precision calculations of $B \to K^*$ form factors from SCET sum rules beyond leading-power contributions

Jing Gao,[1] Ulf-G. Meißner,[1,2,3] Yue-Long Shen,[4] and Dong-Hao Li[5,*]

[1]*Helmholtz-Institut für Strahlen- und Kernphysik and Bethe Center for Theoretical Physics, Universität Bonn, D-53115 Bonn, Germany*

[2]*Institute for Advanced Simulation, Forschungszentrum Jülich, D-52425 Jülich, Germany*

[3]*Peng Huanwu Collaborative Center for Research and Education, International Institute for Interdisciplinary and Frontiers, Beihang University, Beijing 100191, China*

[4]*College of Physics and Photoelectric Engineering, Ocean University of China, Qingdao 266100, China*

[5]*MOE Frontiers Science Center for Rare Isotopes, and School of Nuclear Science and Technology, Lanzhou University, Lanzhou 730000, China*

(Received 21 April 2025; accepted 24 June 2025; published 21 July 2025)

We construct light cone sum rules (LCSR) for the $B \to K^*$ form factors in the large recoil region using vacuum-to-B-meson correlation functions, and systematically calculate subleading-power corrections to these form factors at tree level, including next-to-leading power contributions from the hard-collinear propagator, the subleading effective current $\bar{q}\Gamma[i\not{D}_\perp/(2m_b)]h_v$, and twist-five/six four-particle higher-twist effects. By incorporating the available leading-power results at $\mathcal{O}(\alpha_s)$ and the corrections to higher-twist B-meson light cone distribution amplitudes from our previous work, we improve the precision of theoretical predictions for $B \to K^*$ form factors and find that the subleading-power contributions amount to 30% of the corresponding leading-power results. Employing the Bourrely-Caprini-Lellouch parametrization, we determine the numerical results for $B \to K^*$ form factors across the full kinematic range through a combined fit of LCSR predictions in the large recoil region and lattice QCD results in the small recoil region. Using the newly obtained $B \to K^*$ form factors, we compute the branching fractions for the rare decays $B \to K^*\nu_\ell\bar{\nu}_\ell$ in the Standard Model, obtaining $\mathcal{BR}(\bar{B}^0 \to \bar{K}^{*0}\nu_\ell\bar{\nu}_\ell) = 8.09(96) \times 10^{-6}$ and $\mathcal{BR}(\bar{B}^+ \to \bar{K}^{*+}\nu_\ell\bar{\nu}_\ell) = 9.95(1.05) \times 10^{-6}$. Additionally, we predict that the longitudinal K^* polarization fraction is $F_L = 0.44(4)$.

DOI: 10.1103/yvjd-2ymn

I. INTRODUCTION

The semileptonic B decays induced by the flavor-changing neutral current (FCNC) and accompanied by clean experimental signals, serve as powerful probes of physics beyond the Standard Model (SM). In the prominent semileptonic $b \to s\ell^+\ell^-$ decays, several flavor anomalies have been observed, including a 4.0σ deviation in the experimentally measured $\mathcal{BR}(B^+ \to K^+\mu^+\mu^-)$ compared to the Standard Model predictions in the low q^2 region, where q denotes the momentum of the lepton pair, and the discrepancy between the angular observable $P_5'(B \to K^{*0}\mu^+\mu^-)$ measured by the LHCb Collaboration and the SM predictions in two q^2 bins [1–3]. Notably, the branching ratio of $B \to K\nu_\ell\bar{\nu}_\ell$ reported by the Belle II Collaboration exceeds the Standard Model prediction by 2.7σ [4]. B-meson decays with a pair of neutrinos in the final state are one of the cleanest channels in the SM, since the electroweak effects in these processes are under control and the QCD effects are fully encoded in the corresponding hadronic form factors. Meanwhile, the $b \to s\ell^+\ell^-$ decays are affected by various "nonfactorizable" contributions, including the short-distance hard spectator scattering [5,6], weak annihilation effects [7], and the power-suppressed long-distance quark loop contribution [5,8,9]. Studying the $b \to s\nu\bar{\nu}$ process also allows us to distinguish among different Z' models introduced to explain the anomalies in $b \to s\ell^+\ell^-$, or further constrain the Wilson coefficients of high-dimensional operators within the Standard Model effective field theory [10–12].

In order to make precise theoretical predictions for observables in $B \to K^*\nu_\ell\bar{\nu}_\ell$ decay, precision calculations of $B \to K^*$ form factors are of paramount importance. In the high q^2 region, the form factors have been computed using lattice QCD simulations in Refs. [13,14] and extrapolated to the entire kinetic region. In the low q^2

*Contact author: lidh@lzu.edu.cn

region, several QCD based methods have been developed to derive the factorization formulas involved in the heavy-to-light transition processes with the help of the heavy quark expansion. At leading power in $\Lambda_{\rm QCD}/m_Q$, the seven $B \to V$ form factors can be expressed as a product of the four effective operators in soft-collinear effective theory (SCET), the so-called A0-type and B1-type SCET form factors, and corresponding coefficient functions with hard fluctuations [15–19],

$$\mathcal{F}_i^{B\to V}(n\cdot p) = C_i^{(\mathrm{A0})}(n\cdot p)\xi_a(n\cdot p) + \int d\tau C_i^{(\mathrm{B1})}(\tau, n\cdot p)\Xi_a(\tau, n\cdot p), \quad (a = \parallel, \perp), \tag{1}$$

where $C_i^{(\mathrm{A0})}$ and $C_i^{(\mathrm{B1})}$ are the hard functions corresponding to A0-type and B1-type operators, respectively, with their explicit expressions up to $\mathcal{O}(\alpha_s)$ provided in Appendix A [20–23]. Specifically, $a = \parallel$ for $\mathcal{F}_i^{B\to V} \in \{\mathcal{A}_0, \mathcal{A}_{12}, \mathcal{T}_{23}\}$ and $a = \perp$ for $\mathcal{F}_i^{B\to V} \in \{\mathcal{V}, \mathcal{A}_1, \mathcal{T}_1, \mathcal{T}_2\}$. Owing to the endpoint divergences arising in the convolution of the jet functions and the light cone distribution amplitudes, the soft-collinear factorization of form factors ξ_a cannot be directly accessed. In contrast, the B1-type effective matrix elements can be expressed as the convolution of jet functions and hadronic distribution amplitudes.

Starting from the vacuum-to-light-meson correlation functions with heavy meson interpolating current, light cone sum rules (LCSRs) with light-meson distribution amplitudes has been used to study the $B \to V$ form factors up to twist-four at tree level and to twist-two at $\mathcal{O}(\alpha_s)$ in Refs. [24–27]. Following the analogous strategies, the light cone sum rules for $B \to V$ form factors with B-meson light cone distribution amplitudes at tree level were constructed in Ref. [28], and the subleading-power corrections up to twist-four at tree level were calculated in Ref. [29]. The next-to-leading-logarithmic contribution with SCET sum rules was studied in Ref. [30]. The power corrections to $B \to V$ form factors from two-particle and three-particle higher-twist B-meson light cone distribution amplitudes (LCDAs) have been computed in Ref. [31]. These computations rely on the universal B-meson distribution amplitudes with duality assumption of the light-meson channel and the narrow-width approximation for the vector mesons [32,33]. The finite-width effects in the $B \to K^*$ form factors were investigated in Refs. [34,35]. Compared to QCD factorization, the LCSR approach eliminates the endpoint singularity but introduces a systematic uncertainty due to the quark-hadron duality assumption above a continuum threshold s_0, which is used to determine the lowest-lying hadronic parameters.

This work aims to systematically investigate the subleading-power effects of $B \to K^*$ form factors in QCD by constructing sum rules with B-meson LCDAs, following the approach adopted in Refs. [36–38]. The subleading-power corrections explored in the present work arise from three distinct sources: (I) the power-suppressed terms from the heavy quark expansion (HQE) of the hard-collinear propagator, (II) the subleading effective current $\bar{q}\Gamma[i\not{D}_\perp/(2m_b)]h_v$ from the weak current $\bar{q}\Gamma b$, and (III) the twist-five and twist-six four-body higher-twist contributions. By performing combined fits with lattice QCD results in the high q^2 region and the improved LCSR form factors in the low q^2 region with the Bourrely-Caprini-Lellouch (BCL) parametrization [39–41], we determine the central values and correlation matrix of the BCL z-expansion coefficients. We then explore the observables in the $\bar{B} \to \bar{K}^*\nu_\ell\bar{\nu}_\ell$ process, including the differential branching ratios and the longitudinal K^* polarization fraction.

The organization of the article is as follows: In Sec. II, we present the definitions, notations, and leading power effective SCET form factors at $\mathcal{O}(\alpha_s)$. In Sec. III, we show the computation of various power-suppressed contributions up to twist-six and provide the corresponding $B \to K^*$ form factors in the low q^2 region with LCSR. In Sec. IV, we apply the BCL parametrization in order to get the $B \to K^*$ form factors in the entire momentum region, and determine the z-series expansion coefficients and their correlation matrix by a combined fit of form factors from lattice QCD and LCSR. The updated predictions for the branching ratio $\bar{B} \to \bar{K}^*\nu_\ell\bar{\nu}_\ell$ and longitudinal K^* polarization fraction are also provided. Finally, we discuss our results and future prospects in Sec. V. Various technical details are collected in the Appendixes.

II. NLL CORRECTION TO THE $B \to K^*$ FORM FACTORS AT LEADING POWER

According to the standard Lorentz decomposition of the bilinear quark currents, the $B \to K^*$ form factors are defined in the standard way [15]:

$$
\begin{aligned}
c_V\langle V(p,\varepsilon^*)|\bar{q}\gamma_\mu b|\bar{B}(p+q)\rangle &= -\frac{2iV(q^2)}{m_B+m_V}\epsilon_{\mu\nu\rho\sigma}\varepsilon^{*\nu}p^\rho q^\sigma,\\
c_V\langle V(p,\varepsilon^*)|\bar{q}\gamma_\mu\gamma_5 b|\bar{B}(p+q)\rangle &= \frac{2m_V\varepsilon^*\cdot q}{q^2}q_\mu A_0(q^2)+(m_B+m_V)\left(\varepsilon_\mu^*-\frac{\varepsilon^*\cdot q}{q^2}q_\mu\right)A_1(q^2)\\
&\quad -\frac{\varepsilon^*\cdot q}{m_B+m_V}\left[(2p+q)_\mu-\frac{m_B^2-m_V^2}{q^2}q_\mu\right]A_2(q^2),\\
c_V\langle V(p,\varepsilon^*)|\bar{q}i\sigma_{\mu\nu}q^\nu b|\bar{B}(p+q)\rangle &= -2iT_1(q^2)\epsilon_{\mu\nu\rho\sigma}\varepsilon^{*\nu}p^\rho q^\sigma,\\
c_V\langle V(p,\varepsilon^*)|\bar{q}i\sigma_{\mu\nu}\gamma_5 q^\nu b|\bar{B}(p+q)\rangle &= T_2(q^2)[(m_B^2-m_V^2)\varepsilon_\mu^*-(\varepsilon^*\cdot q)(2p+q)_\mu]\\
&\quad +T_3(q^2)(\varepsilon^*\cdot q)\left[q_\mu-\frac{q^2}{m_B^2-m_V^2}(2p+q)_\mu\right],
\end{aligned}
\tag{2}
$$

with the convention $\epsilon_{0123}=-1$. The factor c_V denotes the flavor structure of a vector meson with $c_V=1$ for the K^* meson. Additionally, m_V and m_B denote the mass of the K^* meson and B meson, respectively. p and q correspond to the momentum of the K^* meson and the momentum transfer of weak current, respectively, with $q=p_B-p=m_B v-p$.

In the following subsection, the calligraphic form factors $\mathcal{F}_i$ represent the linear combinations of the conventionally defined form factors in Eq. (2):

$$
\begin{aligned}
&\mathcal{V}(q^2)=\frac{m_B}{m_B+m_V}V(q^2), \qquad \mathcal{A}_0(q^2)=\frac{m_V}{E_V}A_0(q^2), \qquad \mathcal{A}_1(q^2)=\frac{m_B+m_V}{2E_V}A_1(q^2),\\
&\mathcal{A}_2(q^2)=\frac{m_B-m_V}{m_B}A_2(q^2), \qquad \mathcal{T}_1(q^2)=T_1(q^2), \qquad \mathcal{T}_2(q^2)=\frac{m_B}{2E_V}T_2(q^2),\\
&\mathcal{A}_{12}(q^2)=\mathcal{A}_1(q^2)-\mathcal{A}_2(q^2), \qquad \mathcal{T}_{23}(q^2)=\mathcal{T}_2(q^2)-T_3(q^2).
\end{aligned}
\tag{3}
$$

Following the procedure outlined in Refs. [30,42–44], we can construct the vacuum-to-B-meson correlation functions as follows:

$$
\begin{aligned}
\Pi^{(a)}_{\nu\mu,\parallel}(p,q) &= \int d^4x e^{ip\cdot x}\langle 0|T\{j_\nu(x),\bar{q}(0)\Gamma^{(a)}_\mu b(0)\}|\bar{B}\rangle,\\
\Pi^{(a)}_{\nu\delta\mu,\perp}(p,q) &= \int d^4x e^{ip\cdot x}\langle 0|T\{j_{\nu\delta}(x),\bar{q}(0)\Gamma^{(a)}_\mu b(0)\}|\bar{B}\rangle,
\end{aligned}
\tag{4}
$$

where $j_\nu(x)=\bar{q}'(x)\gamma_\nu q(x)$ and $j_{\nu\delta}(x)=\bar{q}'(x)\gamma_\nu\gamma_{\delta\perp}q(x)$ are the interpolating currents corresponding to the longitudinal and transverse polarization vector meson states with momentum p, respectively. The superscript (a) denotes different Dirac structures. We further introduce two light cone vectors n_μ and $\bar{n}_\mu$, which satisfy the relations $n\cdot\bar{n}=2$ and $n^2=\bar{n}^2=0$. In this work we do not intend to study the power-suppressed contribution arising from the interpolating currents; therefore we keep the leading-power term of the interpolating currents in our calculations. Subsequently, the correlation functions in Eq. (4) can be expressed as

$$
\Pi^{(a)}_{\nu\mu,\parallel}(p,q)=\bar{n}_\nu\Pi^{(a)}_{\mu,\parallel}(p,q), \Pi^{(a)}_{\nu\delta\mu,\perp}(p,q)=\bar{n}_\nu\Pi^{(a)}_{\delta\mu,\perp}(p,q),
\tag{5}
$$

with

$$
\begin{aligned}
\Pi^{(a)}_{\mu,\parallel}(p,q) &= \int d^4x e^{ip\cdot x}\langle 0|T\{\bar{q}'(x)\frac{\not{n}}{2}q(x),\bar{q}(0)\Gamma^{(a)}_\mu b(0)\}\\
&\quad\times|\bar{B}(p+q)\rangle,\\
\Pi^{(a)}_{\delta\mu,\perp}(p,q) &= \int d^4x e^{ip\cdot x}\langle 0|T\{\bar{q}'(x)\frac{\not{n}}{2}\gamma_{\delta\perp}q(x),\bar{q}(0)\Gamma^{(a)}_\mu b(0)\}\\
&\quad\times|\bar{B}(p+q)\rangle.
\end{aligned}
\tag{6}
$$

For convenience, we conduct our research in the rest frame of the B meson, which allows us to express the four-velocity vector of the B meson as $v_\mu=p_B/m_B=(n_\mu+\bar{n}_\mu)/2$. In addition, the power counting scheme for the momentum of interpolating currents, as well as the masses of strange quark is assigned to

$$
\begin{aligned}
&n\cdot p\sim\mathcal{O}(m_b), \qquad |\bar{n}\cdot p|\sim\mathcal{O}(\Lambda_{\rm QCD}/m_b),\\
&m_q\sim m_{q'}\sim\mathcal{O}(\Lambda_{\rm QCD}/m_b).
\end{aligned}
\tag{7}
$$

The correlation functions defined in Eq. (4) can be systematically calculated within the framework of SCET. Since the momentum of the interpolation current is spacelike, there is no endpoint singularity in the convolution integral between the perturbation function and the B-meson distribution

amplitudes, which guarantees factorization of the correlation function. The two-particle leading-twist B-meson LCDA is defined in terms of the nonlocal operators in $\mathrm{SCET_{II}}$ [15,45]:

$$\begin{aligned}\langle 0|(\bar{q}_s Y_s)_\beta(t\bar{n})(Y_s^\dagger h_v)_\alpha(0)|\bar{B}_v\rangle &= -\frac{i\tilde{f}_B(\mu)m_B}{4}\left\{\frac{1+\not{v}}{2}[2\tilde{\phi}_B^+(t,\mu)\right. \\ &\left.+(\tilde{\phi}_B^-(t,\mu)-\tilde{\phi}_B^+(t,\mu))\not{\bar{n}}]\gamma_5\right\}_{\alpha\beta},\end{aligned} \tag{8}$$

where

$$\tilde{\phi}_B^\pm(t) \equiv \int_0^\infty d\omega e^{-i\omega\cdot t}\phi_B^\pm(\omega). \tag{9}$$

The scale-dependent decay constant $\tilde{f}_B(\mu)$ in Heavy Quark Effective Theory (HQET) is related to the decay constant f_B in QCD by the following relation [46]:

$$\tilde{f}_B(\mu) = f_B\left[1-\frac{\alpha_s C_F}{4\pi}\left(3\ln\frac{m_b}{\mu}-2\right)+\mathcal{O}(\alpha_s^2)\right]. \tag{10}$$

$\mathrm{SCET_{II}}$ is an infrared effective theory, which contains only soft and collinear fields (in this work it is equivalent to HQET since no collinear field is taken into account), and it describes all the long distance degrees of freedom. There also exist quark and gluon fields at intermediate scale called hard-collinear scale that is described by $\mathrm{SCET_I}$ operators, which deals with the interaction between hard-collinear and soft fields. The hard-collinear field is at the perturbation region, and should be integrated out to obtain the jet function. Therefore, we need to perform the two-step matching process $\mathrm{QCD} \to \mathrm{SCET_I} \to SCET_{\mathrm{II}}$, and then the perturbation functions, including the hard function and jet function, can be obtained step by step.

Matching the QCD heavy-to-light current to $\mathrm{SCET_I}$ operators, which can contribute to the correlation function at leading power, is shown as follows (see Ref. [21] for the explicit expressions of the A-type and B-type SCET operators):

$$\begin{aligned}(\bar{\psi}\Gamma_i Q)(0) = &\int d\hat{s}\sum_j \tilde{C}_{ij}^{(\mathrm{A0})}(\hat{s})O_j^{(\mathrm{A0})}(s;0) \\ &+\int d\hat{s}\sum_j \tilde{C}_{ij\mu}^{(\mathrm{A1})}(\hat{s})O_j^{(\mathrm{A1})\mu}(s;0) \\ &+\int d\hat{s}_1\int d\hat{s}_2\sum_j \tilde{C}_{ij\mu}^{(\mathrm{B1})}(\hat{s}_1,\hat{s}_2)O_j^{(\mathrm{B1})\mu}(s_1,s_2;0) \\ &+\cdots,\end{aligned} \tag{11}$$

where the hard functions $\tilde{C}_{ij}^{(\mathrm{A0})}(s)$ and $\tilde{C}_{ij\mu}^{(\mathrm{B1})}(\hat{s}_1,\hat{s}_2)$ are given in position space; they could be transformed into momentum space through Fourier transformation, and the corresponding momentum space hard function is written by $C_i^{(\mathrm{A0})}(n\cdot p,\mu)$ and $C_i^{(\mathrm{B1})}(n\cdot p,\tau,\mu)$. Because the hard functions $C_i^{(\mathrm{A0})}$ and $C_i^{(\mathrm{B1})}$ contain the enhanced logarithms $\ln^n(m_b/\Lambda_{\mathrm{QCD}})$, they should be summed up to all orders in perturbation theory with Next-to-Leading Logarithmic (NLL) and Leading Logarithmic (LL) accuracy by solving the renormalization equation [20,21]. The general solutions to the RG equations are

$$C_i^{(\mathrm{A0})}(n\cdot p,\mu) = U_1(n\cdot p,\mu_h,\mu)C_i^{(\mathrm{A0})}(n\cdot p,\mu_h), \tag{12}$$

$$\begin{aligned}C_i^{(\mathrm{B1})}(n\cdot p,\tau,\mu) = &\exp[-S(n\cdot p,\mu_h,\mu)] \\ &\times\int_0^1 d\tau' U_i^{(\mathrm{B1})}(\tau,\tau',\mu_h,\mu) \\ &\times C_i^{(\mathrm{B1})}(n\cdot p,\tau',\mu_h),\end{aligned} \tag{13}$$

where the NLL resummation evolution factor U_1 and LL expansion of the S function are detailed in Refs. [21,46]. The jet function can be obtained by matching the matrix element of the time-ordered product of $\mathrm{SCET_I}$ operators and the $\mathrm{SCET_I}$ Lagrangian [47] to the matrix elements of $\mathrm{SCET_{II}}$ operators. In practical operation, one can just evaluate the Feynman diagrams in Fig. 1 for the tree-level result, and the $\mathcal{O}(\alpha_s)$ contribution has been calculated in Ref. [31]. To extract the form factors of the $B\to K^*$ process, we utilize a dispersion relation and express the partonic correlation function as a dispersion integral [48],

$$\Pi(n\cdot p,\bar{n}\cdot p) = \frac{1}{\pi}\int_0^\infty d\omega' \frac{\mathrm{Im}\,\Pi(n\cdot p,\omega')}{\omega'-\bar{n}\cdot p-i\epsilon}. \tag{14}$$

At the hadronic level, the correlation function with different interpolating currents can be expressed by the following formulas:

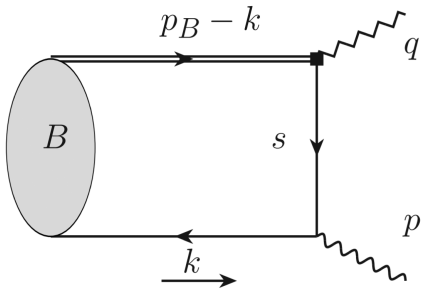

FIG. 1. Diagrammatic representations of the vacuum-to-B-meson correlation functions at tree level, where the double line stands for the effective heavy quark field in HQET, the wave line indicates the interpolating current, and the square box denotes the weak vertex.

$$\Pi^{(\mathrm{V-A})}_{\mu,\parallel}(p,q) = \frac{f_V^{\parallel} m_V}{m_V^2/n\cdot p - \bar{n}\cdot p - i0}\left(\frac{n\cdot p}{2m_V}\right)^2 \Bigg\{\frac{m_B}{m_B - n\cdot p} n_\mu \Bigg[\left(-\frac{2m_V}{n\cdot p}A_0(q^2)\right) + \left(\frac{m_B+m_V}{n\cdot p}A_1(q^2) - \frac{m_B - m_V}{m_B}A_2(q^2)\right)\Bigg] - \bar{n}_\mu\Bigg[\left(\frac{2m_V}{n\cdot p}A_0(q^2)\right) + \left(\frac{m_B+m_V}{n\cdot p}A_1(q^2) - \frac{m_B-m_V}{m_B}A_2(q^2)\right)\Bigg]\Bigg\} + \int d\omega' \frac{1}{\omega' - \bar{n}\cdot p - i0}\left[n_\mu \varrho^{(\mathrm{V-A})}_{n,\parallel}(\omega', n\cdot p) + \bar{n}_\mu \varrho^{(\mathrm{V-A})}_{\bar{n},\parallel}(\omega', n\cdot p)\right], \tag{15}$$

$$\Pi^{(\mathrm{V-A})}_{\delta\mu,\perp}(p,q) = -\frac{1}{2}\frac{f_V^{\perp} n\cdot p}{m_V^2/n\cdot p - \bar{n}\cdot p - i0}\times\left[g^{\perp}_{\delta\mu}\left(\frac{m_B+m_V}{n\cdot p}A_1(q^2)\right) + i\epsilon^{\perp}_{\delta\mu}\left(\frac{m_B}{m_B+m_V}V(q^2)\right)\right] + \int d\omega' \frac{1}{\omega' - \bar{n}\cdot p - i0}\left[g^{\perp}_{\delta\mu}\varrho^{(\mathrm{V-A})}_{\perp,A_1}(\omega', n\cdot p) + i\epsilon^{\perp}_{\delta\mu}\varrho^{(\mathrm{V-A})}_{\perp,V}(\omega', n\cdot p)\right], \tag{16}$$

$$\Pi^{(\mathrm{T+\tilde{T}})}_{\mu,\parallel}(p,q) = \frac{1}{2}\frac{f_V^{\parallel} m_V}{m_V^2/n\cdot p - \bar{n}\cdot p - i0}\left(\frac{n\cdot p}{2m_V}\right)^2 [n\cdot q\bar{n}_\mu - \bar{n}\cdot q n_\mu]\left[\frac{m_B}{n\cdot p}T_2(q^2) - T_3(q^2)\right] + \int d\omega' \frac{1}{\omega' - \bar{n}\cdot p - i0}[n\cdot q\bar{n}_\mu - \bar{n}\cdot q n_\mu]\varrho^{(\mathrm{T+\tilde{T}})}_{\parallel}(\omega', n\cdot p), \tag{17}$$

$$\Pi^{(\mathrm{T+\tilde{T}})}_{\delta\mu,\perp}(p,q) = \frac{1}{2}\frac{f_V^{\perp} n\cdot p m_B}{m_V^2/n\cdot p - \bar{n}\cdot p - i0}\left[g^{\perp}_{\delta\mu}\left(\frac{m_B}{n\cdot p}T_2(q^2)\right) + i\epsilon^{\perp}_{\delta\mu}T_1(q^2)\right] + \int d\omega' \frac{1}{\omega' - \bar{n}\cdot p - i0}\left[g^{\perp}_{\delta\mu}\varrho^{(\mathrm{T+\tilde{T}})}_{\perp,T_2}(\omega', n\cdot p) + i\epsilon^{\perp}_{\delta\mu}\varrho^{(\mathrm{T+\tilde{T}})}_{\perp,T_1}(\omega', n\cdot p)\right], \tag{18}$$

where the definitions of decay constants for the longitudinal and transverse K^* meson are given by Ref. [30],

$$\langle 0|\bar{q}'(x)\frac{\not{n}}{2}q(x)|V(p,\varepsilon)\rangle = \frac{i}{2}f_V^{\parallel} m_V n\cdot\varepsilon,$$
$$\langle 0|\bar{q}'(x)\frac{\not{n}}{2}\gamma^{\perp}_{\delta}q(x)|V(p,\varepsilon)\rangle = -n\cdot p\frac{i}{2}f_V^{\perp}\varepsilon^{\perp}_{\delta}(p). \tag{19}$$

At leading power, the large recoil symmetry reduces the seven $B \to V$ form factors to two, namely, $\xi_{\parallel}(n\cdot p)$ and $\xi_{\perp}(n\cdot p)$. The relation between the QCD form factors in the above equation and the SCET form factors $\xi_{\parallel,\perp}(\bar{n}\cdot p)$ can be found in Ref. [31]. Taking advantage of these relations, all the correlation functions can be expressed in terms of the SCET form factors. We then apply quark-hadron duality and Borel transformation to both the partonic and hadronic correlation functions in the SCET representation to eliminate the continuum and resonance contributions, thereby reducing the uncertainties from the duality ansatz. We finally obtain the four effective SCET form factors at $\mathcal{O}(\alpha_s)$ [31]:

$$\xi_{\parallel,\mathrm{NLL}}(n\cdot p) = \frac{U_2(\mu_{h2},\mu)\tilde{f}_B(\mu_{h2})}{f_V^{\parallel}}\frac{2m_B m_V}{(n\cdot p)^2}\int_0^{\omega_s^{\parallel}} d\omega' \exp\left[-\frac{n\cdot p\omega' - m_V^2}{n\cdot p\omega_M}\right][\phi^-_{B,\mathrm{eff}}(\omega',\mu) + \phi^+_{B,m}(\omega',\mu)], \tag{20}$$

$$\xi_{\perp,\mathrm{NLL}}(n\cdot p) = \frac{U_2(\mu_{h2},\mu)\tilde{f}_B(\mu_{h2})}{f_V^{\perp}(\nu)}\frac{m_B}{n\cdot p}\int_0^{\omega_s^{\perp}} d\omega' \exp\left[-\frac{n\cdot p\omega' - m_V^2}{n\cdot p\omega_M}\right]\tilde{\phi}^-_{B,\mathrm{eff}}(\omega',\mu,\nu), \tag{21}$$

$$\Xi_{\parallel,\mathrm{NLL}}(n\cdot p) = -\frac{\alpha_s C_F}{\pi}\frac{U_2(\mu_{h2},\mu)\tilde{f}_B(\mu_{h2})}{f_V^{\parallel}}\frac{m_B m_V}{n\cdot p m_b}[(1-\tau)\theta(\tau)\theta(1-\tau)] \times\int_0^{\omega_s^{\parallel}} d\omega' \exp\left[-\frac{n\cdot p\omega' - m_V^2}{n\cdot p\omega_M}\right]\int_{\omega'}^{\infty} d\omega\frac{\phi_B^+(\omega,\mu)}{\omega}, \tag{22}$$

$$\Xi_{\perp,\mathrm{NLL}}(n\cdot p) = -\frac{\alpha_s C_F}{2\pi}\frac{U_2(\mu_{h2},\mu)\tilde{f}_B(\mu_{h2})}{f_V^{\perp}(\nu)}\frac{m_B}{m_b}[(1-\tau)\theta(\tau)\theta(1-\tau)] \times \int_0^{\omega_s^{\perp}} d\omega' \exp\left[-\frac{n\cdot p\omega' - m_V^2}{n\cdot p\omega_M}\right]\int_{\omega'}^{\infty} d\omega \frac{\phi_B^{+}(\omega,\mu)}{\omega}, \tag{23}$$

where $\omega_s^{\parallel,\perp} = s_0^{\parallel,\perp}/n\cdot p$ and $\omega_M = M^2/n\cdot p$ denote the effective threshold and Borel mass, respectively, which are two fundamental inputs of LCSR. μ and ν correspond to the factorization scale and renormalization scale, respectively. Additionally, the effective B-meson distribution amplitudes are introduced to describe both the hard-collinear and soft fluctuations [31,43,44], as given in Appendix B. The quark mass contributions in SCET have been investigated in Ref. [49], and the leading-power spectator-quark mass corrections to $B_{(s)}$-meson decay form factors at one-loop accuracy have been calculated in Refs. [36,38]. In this work, we do not include the spectator-quark mass corrections to the effective SCET form factors at one-loop accuracy. The omission is justified because the spectator quark in the $B \to K^*$ decay process is either a u quark or d quark, whose mass-induced corrections are significantly suppressed compared to those from the s quark in B_s-meson decays. We will estimate the spectator-quark correction to the $B \to K^*$ form factors with the SCET sum rules in our future work.

III. SUBLEADING-POWER CONTRIBUTIONS

In this section, we investigate the power corrections arising from various sources to the $B \to K^*$ form factors within the LCSR approach. Utilizing the equations of motion in HQET and the factorization formula of correlation functions at subleading power, we ultimately obtain the tree-level power corrections to the $B \to K^*$ form factors in the large hadronic recoil region and analyze the scaling behavior of these form factors.

A. Higher-twist B-meson LCDA contribution

The contributions from the higher-twist B-meson LCDAs of two particle and three particle are shown in Fig. 2. In order to define higher-twist B-meson LCDAs, the general parametrization of the vacuum-to-B-meson matrix element of the three-body HQET operator is given by Ref. [50],

$$\begin{aligned}\langle 0|\bar{q}_\alpha(z_1\bar{n})g_s G^{\mu\nu}(z_2\bar{n})h_{v\beta}|0\rangle =& \frac{\tilde{f}_B(\mu)m_B}{4}[(1+\not{v})\{(v_\mu\gamma_\nu - v_\nu\gamma_\mu)[\Psi_A(z_1,z_2,\mu)-\Psi_V(z_1,z_2,\mu)] \\ & - i\sigma_{\mu\nu}\Psi_V(z_1,z_2,\mu) - (\bar{n}_\mu v_\nu - \bar{n}_\nu v_\mu)X_A(z_1,z_2,\mu) + (\bar{n}_\mu\gamma_\nu - \bar{n}_\nu\gamma_\mu)[W(z_1,z_2,\mu)+Y_A(z_1,z_2,\mu)] \\ & + i\epsilon_{\mu\nu\alpha\beta}\bar{n}^\alpha v^\beta\gamma_5\tilde{X}_A(z_1,z_2,\mu) - i\epsilon_{\mu\nu\alpha\beta}\bar{n}^\alpha\gamma^\beta\gamma_5\tilde{Y}_A(z_1,z_2,\mu) \\ & - (\bar{n}_\mu v_\nu - \bar{n}_\nu v_\mu)\not{\bar{n}}W(z_1,z_2,\mu) + (\bar{n}_\mu\gamma_\nu - \bar{n}_\nu\gamma_\mu)\not{\bar{n}}Z(z_1,z_2,\mu)\}\gamma_5]_{\beta\alpha},\end{aligned} \tag{24}$$

where $\epsilon_{0123} = -1$, and we also introduce three-particle HQET distribution amplitudes of definite collinear twist as follows:

$$\begin{aligned}&\Phi_3 = \Psi_A - \Psi_V, \qquad \Phi_4 = \Psi_A + \Psi_V, \\ &\Psi_4 = \Psi_A + X_A, \qquad \tilde{\Psi}_4 = \Psi_V - \tilde{X}_A, \\ &\tilde{\Phi}_5 = \Psi_A + \Psi_V + 2Y_A - 2\tilde{Y}_A + 2W, \qquad \Psi_5 = -\Psi_A + X_A - 2Y_A, \\ &\tilde{\Psi}_5 = -\Psi_V - \tilde{X}_A + 2\tilde{Y}_A, \qquad \Phi_6 = \Psi_A - \Psi_V + 2Y_A + 2W + 2\tilde{Y}_A - 4Z.\end{aligned} \tag{25}$$

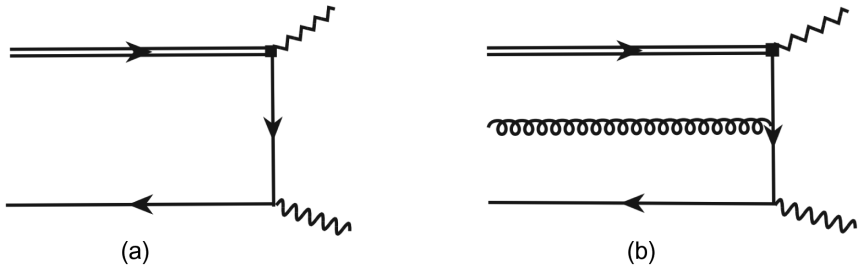

FIG. 2. Diagrammatic representations of two-particle (a) and three-particle (b) corrections to the vacuum-to-B-meson correlation functions at tree level, where the square box indicates the weak vertex and the wavy line represents the interpolating current.

To facilitate the calculation of the contributions from high-twist LCDAs more effectively, we introduce the light cone expansion of the quark propagator within the background gluon field,

$$\langle 0|T\{\bar{q}(x), q(0)\}|0\rangle \supset ig_s \int \frac{d^4l}{(2\pi)^4} e^{-il\cdot x} \int_0^1 du \left[\frac{ux_\mu \gamma_\nu}{l^2 - m_q^2} - \frac{(\not{l} + m_q)\sigma_{\mu\nu}}{2(l^2 - m_q^2)^2}\right] G^{\mu\nu}(ux), \tag{26}$$

which can be found in Ref. [51].

First, we evaluate the correlation function $\Pi_\parallel^{(a)}(p,q)$ in Eq. (6), which corresponds to the longitudinally polarized vector meson. Contracting the quark fields $q(x)$ and $\bar{q}(0)$ [leads to the propagator in Eq. (26)], taking advantage of the three-particle higher-twist B-meson LCDA in Eq. (24), the three-particle higher-twist correction to the correlation function can be written as

$$\Pi_{\parallel,\mathrm{NLP}}^{(a),3\mathrm{PHT}}(p,q) = \frac{\tilde{f}_B(\mu) m_B}{2n\cdot p}[\Gamma_\parallel^{(a)} \Pi_{\parallel,\mathrm{NLP}}^{3\mathrm{PHT}} + \tilde{\Gamma}_\parallel^{(a)} \tilde{\Pi}_{\parallel,\mathrm{NLP}}^{3\mathrm{PHT}}], \tag{27}$$

with

$$\begin{aligned}
\Pi_{\parallel,\mathrm{NLP}}^{3\mathrm{PHT}} &= \int_0^\infty d\omega_1 \int_0^\infty d\omega_2 \int_0^1 du \frac{-2\bar{u}\Phi_4(\omega_1,\omega_2)}{(\bar{n}\cdot p - \omega_1 - u\omega_2 - \omega_q)^2} + \frac{m_q}{n\cdot p}\frac{\Psi_5(\omega_1,\omega_2) - \tilde{\Psi}_5(\omega_1,\omega_2)}{(\bar{n}\cdot p - \omega_1 - u\omega_2 - \omega_q)^2}, \\
\tilde{\Pi}_{\parallel,\mathrm{NLP}}^{3\mathrm{PHT}} &= \int_0^\infty d\omega_1 \int_0^\infty d\omega_2 \int_0^1 du \frac{\tilde{\Psi}_5(\omega_1,\omega_2) - (2u-1)\Phi_5(\omega_1,\omega_2)}{(\bar{n}\cdot p - \omega_1 - u\omega_2 - \omega_q)^2} - \frac{m_q}{n\cdot p}\frac{2\tilde{\Phi}_6(\omega_1,\omega_2)}{(\bar{n}\cdot p - \omega_1 - u\omega_2 - \omega_q)^2},
\end{aligned} \tag{28}$$

where the factors $\Gamma_\parallel^{(a)}$ and $\tilde{\Gamma}_\parallel^{(a)}$ take the form

$$\{\Gamma_\parallel^{(\mathrm{V-A})}, \Gamma_\parallel^{(\mathrm{T+\tilde{T}})}\} \in \left\{n_\mu, \bar{n}_\mu \frac{n\cdot q}{2} - n_\mu \frac{\bar{n}\cdot q}{2}\right\}, \qquad \{\tilde{\Gamma}_\parallel^{(\mathrm{V-A})}, \Gamma_\parallel^{(\mathrm{T+\tilde{T}})}\} \in \left\{\bar{n}_\mu, n_\mu \frac{\bar{n}\cdot q}{2} - \bar{n}_\mu \frac{n\cdot q}{2}\right\}, \tag{29}$$

and $a \in \{\mathrm{V-A}, \mathrm{T+\tilde{T}}\}$ denotes the different Dirac structures $\gamma_\mu(1-\gamma_5)$ and $i\sigma_{\mu\nu}(1+\gamma_5)q^\nu$ of the heavy-to-light weak current, respectively. Additionally, we set $\omega_q = m_q^2/n\cdot p$ for brevity.

Along the same lines, the three-particle higher-twist correction to the correlation function $\Pi_\perp^{(a)}(p,q)$ in Eq. (6), which corresponds to a transversely polarized vector meson, can be expressed as

$$\begin{aligned}
\Pi_{\perp,\mathrm{NLP}}^{(a),3\mathrm{PHT}}(p,q) = \frac{\tilde{f}_B(\mu) m_B}{2n\cdot p} \int_0^\infty d\omega_1 \int_0^\infty d\omega_2 \int_0^1 du \Bigg[&\Gamma_\perp^{(a)} \frac{(1-2u)\Psi_5(\omega_1,\omega_2) - \tilde{\Psi}_5(\omega_1,\omega_2)}{(\bar{n}\cdot p - \omega_1 - u\omega_2 - \omega_q)^2} \\
&- \tilde{\Gamma}_\perp^{(a)} \frac{m_q}{n\cdot p}\frac{\Psi_5(\omega_1,\omega_2) + \tilde{\Psi}_5(\omega_1,\omega_2)}{(\bar{n}\cdot p - \omega_1 - u\omega_2 - \omega_q)^2}\Bigg]
\end{aligned} \tag{30}$$

by taking $\epsilon_{\delta\mu}^\perp \equiv \frac{1}{2}\epsilon_{\delta\mu\rho\sigma} n^\rho \bar{n}^\sigma$ and

$$\{\Gamma_\perp^{(\mathrm{V-A})}, \Gamma_\perp^{(\mathrm{T+\tilde{T}})}\} \in \{g_{\delta\mu}^\perp + i\epsilon_{\delta\mu}, g_{\delta\mu}^\perp - i\epsilon_{\delta\mu}^\perp\}, \quad \{\tilde{\Gamma}_\perp^{(\mathrm{V-A})}, \tilde{\Gamma}_\perp^{(\mathrm{T+\tilde{T}})}\} \in -\{\bar{n}\cdot q(g_{\delta\mu}^\perp + i\epsilon_{\delta\mu}), n\cdot q(g_{\delta\mu}^\perp - i\epsilon_{\delta\mu}^\perp)\}. \tag{31}$$

In addition, the two-particle higher-twist B-meson LCDAs, for example $g_B^\pm(\omega)$, also generate subleading-power contributions. The off-light cone corrections to the renormalized two-body nonlocal HQET matrix element at $\mathcal{O}(x^2)$ accuracy is given by Ref. [50]:

$$\begin{aligned}
\langle 0|(\bar{q}_s Y_s)_\beta(x)(Y_s^\dagger h_v)_\alpha|\bar{B}_v\rangle = -i\frac{\tilde{f}_B(\mu) m_B}{4} \int_0^\infty d\omega e^{-i\omega v\cdot x} \Bigg[&\frac{1+\not{v}}{2}\{2[\phi_B^+(\omega,\mu) + x^2 g_B^+(\omega,\mu)] \\
&- \frac{\not{x}}{v\cdot x}[(\phi_B^+(\omega,\mu) - \phi_B^-(\omega,\mu)) + x^2(g_B^+(\omega,\mu) - g_B^-(\omega,\mu))]\}\gamma_5\Bigg]_{\alpha\beta},
\end{aligned} \tag{32}$$

where the higher-twist LCDA $g_B^-(\omega,\mu)$ can be decomposed into the "genuine" twist-five three-particle LCDA $\Psi_5(\omega_1,\omega_2,\mu)$ and the lower-twist "Wandzura-Wilczek" two-particle LCDA $\hat{g}_B^-(\omega,\mu)$,

$$g_B^-(x)=\hat{g}_B^-(x)-\frac{1}{2}\int_0^1 du\bar{u}\Psi_5(x,ux). \tag{33}$$

After inserting the two-particle higher-twist B-meson LCDAs given in Eq. (32) into the correlation functions, we obtain the factorization formulas for the two-particle higher-twist contributions

$$\Pi_{\parallel,\perp}^{(a),\mathrm{2PHT}}(p,q)=\frac{\tilde{f}_B(\mu)m_B}{2n\cdot p}\Gamma_{\parallel,\perp}^{(a)}\left\{\int_0^\infty d\omega\frac{4\hat{g}_B^-(\omega,\mu)}{(\bar{n}\cdot p-\omega)^2}-\int_0^\infty d\omega_1\int_0^\infty d\omega_2\int_0^1 du\frac{2\bar{u}\Psi_5(\omega_1,\omega_2)}{(\bar{n}\cdot p-\omega_1-u\omega_2)^2}\right\}, \tag{34}$$

with $\Gamma_\parallel^{(a)}\in\{\bar{n}_\mu,n_\mu\frac{\bar{n}\cdot q}{2}-\bar{n}_\mu\frac{n\cdot q}{2}\}$ and $\Gamma_\perp^{(a)}\in\{g_{\delta\mu}^\perp+i\epsilon_{\delta\mu}^\perp,-\bar{n}\cdot q(g_{\delta\mu}^\perp+i\epsilon_{\delta\mu}^\perp)\}$ for $a\in\{\mathrm{V}-\mathrm{A},\mathrm{T}+\tilde{\mathrm{T}}\}$.

Summing up the two-particle and three-particle higher-twist contributions, we obtain the higher-twist corrections to the correlation functions $\Pi_{\parallel,\perp}^{(a)}(p,q)$ at tree level. We then implement the dispersion relation to the correlation functions at the partonic level and apply the quark-hadron duality ansatz and Borel transformation. This procedure yields the following sum rules for the higher-twist corrections to the $B\to K^*$ form factors [31]:

$$\begin{aligned}
&f_V^\perp\exp\left[-\frac{m_V^2}{n\cdot p\omega_M}\right]\{\mathcal{V}_{\mathrm{NLP}}^{\mathrm{HT}}(q^2),\mathcal{A}_{1,\mathrm{NLP}}^{\mathrm{HT}}(q^2),\mathcal{T}_{1,\mathrm{NLP}}^{\mathrm{HT}}(q^2),\mathcal{T}_{2,\mathrm{NLP}}^{\mathrm{HT}}(q^2)\}\\
&\quad=\frac{\tilde{f}_B(\mu)m_B}{(n\cdot p)^2}\left\{f_{2,1}[\boldsymbol{\tau}_1]+f_{3,2}[\boldsymbol{\tau}_2]-\kappa_i\frac{m_q}{n\cdot p}f_{3,2}[\boldsymbol{\tau}_2]\right\},\\
&f_V^\parallel\exp\left[-\frac{m_V^2}{n\cdot p\omega_M}\right]\{\mathcal{A}_{0,\mathrm{NLP}}^{\mathrm{HT}}(q^2),\mathcal{A}_{12,\mathrm{NLP}}^{\mathrm{HT}}(q^2),\mathcal{T}_{23,\mathrm{NLP}}^{\mathrm{HT}}(q^2)\}\\
&\quad=\frac{2\tilde{f}_B(\mu)m_Bm_V}{(n\cdot p)^3}\left\{f_{2,1}[\boldsymbol{\tau}_1]+f_{3,2}[\boldsymbol{\tau}_3]+\frac{m_q}{n\cdot p}f_{3,2}[\boldsymbol{\tau}_4]+\iota_i\left(f_{3,2}[\boldsymbol{\tau}_5]+\frac{m_q}{n\cdot p}f_{3,2}[-\boldsymbol{\tau}_3]\right)\right\},
\end{aligned} \tag{35}$$

with the symmetry-breaking factors

$$\kappa_i\in\left\{+1,-1,\frac{n\cdot q}{\bar{n}\cdot q},-\frac{n\cdot q}{\bar{n}\cdot q}\right\},\quad \iota_i\in\left\{\frac{n\cdot q}{m_B},-\frac{n\cdot q}{m_B},-1\right\}, \tag{36}$$

where the function $f_{i,j}$ describes the contribution of terms in the form $\phi(\omega)/(\omega-\cdots)^j$, with $\phi(\omega)$ being the i-particle LCDA and the denominator raised to the j-th power. The explicit expressions of $f_{i,j}$ are listed in Appendix C, and the density functions are expressed by

$$\begin{aligned}
&\boldsymbol{\tau}_1(\omega)=4\frac{d}{d\omega}\hat{g}_B^-(\omega),\qquad \boldsymbol{\tau}_2(\omega_1,\omega_2,u)=\Psi_5(\omega_1,\omega_2)+\tilde{\Psi}_5(\omega_1,\omega_2),\\
&\boldsymbol{\tau}_3(\omega_1,\omega_2,u)=\Psi_5(\omega_1,\omega_2)-\tilde{\Psi}_5(\omega_1,\omega_2),\qquad \boldsymbol{\tau}_4(\omega_1,\omega_2,u)=2\Phi_6(\omega_1,\omega_2),\\
&\boldsymbol{\tau}_5(\omega_1,\omega_2,u)=2\bar{u}\Phi_4(\omega_1,\omega_2).
\end{aligned} \tag{37}$$

B. Higher-order terms in hard-collinear propagator

Adopting the approach detailed in Refs. [36–38], we carry out the calculation of the subleading power corrections stemming from the hard-collinear propagator in the correlation functions expressed by Eq. (6). Given that the momentum in the interpolating current lies in the hard-collinear regime, the quark propagator connecting this interpolating current and a soft quark also possesses hard-collinear momentum. Expanding the hard-collinear propagator in terms of powers of $\Lambda_{\mathrm{QCD}}/m_b$ gives rise to

$$\frac{\not{p}-\not{k}+m_q}{(p-k)^2-m_q^2+i\epsilon}=\frac{\overbrace{\left[n\cdot p\frac{\not{\bar{n}}}{2}}^{\text{LP}}+\overbrace{(\bar{n}\cdot p\frac{\not{n}}{2}-\not{k}+m_q)+\frac{n\cdot p\frac{\not{n}}{2}\bar{n}\cdot pn\cdot k}{n\cdot p(\bar{n}\cdot p-\bar{n}\cdot k)}+\frac{n\cdot p\frac{\not{n}}{2}(m_q^2-m_{q'}^2)}{n\cdot p(\bar{n}\cdot p-\bar{n}\cdot k)}}^{\text{NLP}}\right]}{n\cdot p(\bar{n}\cdot p-\bar{n}\cdot k)}, \tag{38}$$

where m_q is the mass of the hard-collinear quark propagator and $m_{q'}$ is the mass of the B-meson spectator quark. "LP" refers to the leading-power contribution of hard-collinear propagator at tree level, while "NLP" represents the next-to-leading power contributions resulting from the expansion of the hard-collinear propagator.

We then insert the NLP terms into the correlation functions $\Pi_{\parallel,\perp}^{(a)}$, and apply the HQET operator identities [50,52],

$$\begin{aligned}
v_\rho\frac{\partial}{\partial x_\rho}\bar{q}(x)\Gamma[x,0]h_v(0)&=v\cdot\partial\bar{q}(x)\Gamma[x,0]h_v(0)+i\int_0^1 du\bar{u}\bar{q}(x)[x,ux]x^\lambda g_s G_{\lambda\rho}(ux)[ux,0]v^\rho\Gamma h_v(0),\\
iv\cdot\partial\langle 0|\bar{q}(x)\Gamma[x,0]h_v(0)|\bar{B}_v\rangle&=\bar{\Lambda}\langle 0|\bar{q}(x)\Gamma[x,0]h_v(0)|\bar{B}_v\rangle,\\
\frac{\partial}{\partial x_\rho}\bar{q}(x)\gamma_\rho\Gamma[x,0]h_v(0)&=-i\int_0^1 duu\bar{q}(x)[x,ux]x^\lambda g_s G_{\lambda\rho}(ux)[ux,0]\gamma^\rho\Gamma h_v(0)+im_{q'}\bar{q}(x)\Gamma[x,0]h_v(0).
\end{aligned} \tag{39}$$

Taking advantage of the three-body light cone HQET matrix element up to twist-six accuracy in Eq. (24), we are able to derive the results for the first NLP term presented in Eq. (38),

$$\begin{aligned}
\Pi_{\text{NLP}}^{\text{I,QPE}}&=\left[\frac{\tilde{f}_B(\mu)m_B}{2n\cdot p}\right]\left\{\int_0^\infty d\omega\frac{(\omega-2\bar{\Lambda})\phi_B^+(\omega)}{\bar{n}\cdot p-\omega}+(m_{q'}-m_q)\int_0^\infty d\omega\frac{\phi_B^-(\omega)}{\bar{n}\cdot p-\omega}\right.\\
&\left.-\int_0^1 du\int_0^\infty d\omega_1\int_0^\infty d\omega_2\frac{2[u\Phi_4(\omega_1,\omega_2)+\Psi_4(\omega_1,\omega_2)]}{(\bar{n}\cdot p-\omega_1-u\omega_2)^2}\right\},\\
\tilde{\Pi}_{\text{NLP}}^{\text{I,QPE}}&=\left[\frac{\tilde{f}_B(\mu)m_B}{2n\cdot p}\right]\left\{\int_0^\infty d\omega\frac{(\omega-2\bar{\Lambda})}{\bar{n}\cdot p-\omega}\phi_B^-(\omega)-\int_0^1 du\int_0^\infty d\omega_1\int_0^\infty d\omega_2\frac{2\bar{u}\Psi_5(\omega_1,\omega_2)}{(\bar{n}\cdot p-\omega_1-u\omega_2)^2}\right\},
\end{aligned} \tag{40}$$

where the hadronic parameter $\bar{\Lambda}$ characterizes the "effective mass" of the B-meson state in HQET. It can be defined as [53]

$$\bar{\Lambda}\equiv\frac{\langle 0|\bar{q}iv\cdot\overleftarrow{D}\Gamma h_v|\bar{B}_q(v)\rangle}{\langle 0|\bar{q}i\Gamma h_v|\bar{B}_q(v)\rangle}. \tag{41}$$

Noting the relation $n_\alpha=2v_\alpha-\bar{n}_\alpha$, we can further compute the contribution of the second NLP term along the same lines,

$$\Pi_{\text{NLP}}^{\text{II,QPE}}=0,\quad \tilde{\Pi}_{\text{NLP}}^{\text{II,QPE}}=\left[\frac{\tilde{f}_B(\mu)m_B}{2n\cdot p}\right]\left\{\int_0^\infty d\omega\frac{\bar{n}\cdot p(2\bar{\Lambda}-\omega)}{(\bar{n}\cdot p-\omega)^2}\phi_B^-(\omega)+\int_0^1 du\int_0^\infty d\omega_1\int_0^\infty d\omega_2\frac{4\bar{u}\,\bar{n}\cdot p\Psi_5(\omega_1,\omega_2)}{(\bar{n}\cdot p-\omega_1-u\omega_2)^3}\right\}. \tag{42}$$

Subsequently, the contribution of the third NLP term of the hard-collinear propagator expansion can be easily derived by applying the standard factorization procedure,

$$\Pi_{\text{NLP}}^{\text{III,QPE}}=0,\qquad \tilde{\Pi}_{\text{NLP}}^{\text{III,QPE}}=(m_q^2-m_{q'}^2)\int_0^\infty d\omega\frac{1}{(\bar{n}\cdot p-\omega)^2}\phi_B^-(\omega). \tag{43}$$

Ultimately, we obtain the factorization formulas for the NLP contributions stemming from the quark propagator expansion at tree level:

$$\Pi_{j,\text{NLP}}^{(a),\text{QPE}}=\Gamma_j^{(a)}(\Pi_{\text{NLP}}^{\text{I,QPE}}+\Pi_{\text{NLP}}^{\text{II,QPE}}+\Pi_{\text{NLP}}^{\text{III,QPE}})+\tilde{\Gamma}_j^{(a)}(\tilde{\Pi}_{\text{NLP}}^{\text{I,QPE}}+\tilde{\Pi}_{\text{NLP}}^{\text{II,QPE}}+\tilde{\Pi}_{\text{NLP}}^{\text{III,QPE}}), \tag{44}$$

with

$$\Gamma_{\parallel,\perp}^{(\text{V-A})}=\{n_\mu,g_{\delta\mu}^\perp-i\epsilon_{\delta\mu}^\perp\},\qquad \tilde{\Gamma}_{\parallel,\perp}^{(\text{V-A})}=\{\bar{n}_\mu,g_{\delta\mu}^\perp+i\epsilon_{\delta\mu}^\perp\}, \tag{45}$$

and

$$\Gamma_{\parallel,\perp}^{(\mathrm{T}+\tilde{\mathrm{T}})} = -\left\{ n_\mu \frac{\bar{n}\cdot q}{2} - \bar{n}_\mu \frac{n\cdot q}{2}, (g_{\delta\mu}^{\perp} - i\epsilon_{\delta\mu}^{\perp}) \frac{n\cdot q}{2} \right\},$$
$$\tilde{\Gamma}_{\parallel,\perp}^{(\mathrm{T}+\tilde{\mathrm{T}})} = -\left\{ \bar{n}_\mu \frac{n\cdot q}{2} - n_\mu \frac{\bar{n}\cdot q}{2}, (g_{\delta\mu}^{\perp} + i\epsilon_{\delta\mu}^{\perp}) \frac{\bar{n}\cdot q}{2} \right\}. \quad (46)$$

Adopting the standard LCSR strategy, we formulate the correlation functions in the dispersion relation formalism and match them to the hadronic representation given from Eqs. (15) to (18). Finally, the desired $B \to K^*$ form factors for the power-suppressed contribution stemming from the hard-collinear propagator can be expressed as

$$f_V \exp\left[-\frac{m_V^2}{n\cdot p\omega_M}\right] \mathcal{F}_{i,\mathrm{NLP}}^{\mathrm{QPE}}(q^2)$$
$$= \frac{\tilde{f}_B(\mu) m_B}{(n\cdot p)^2} \{\kappa_i (f_{2,1}[\boldsymbol{\eta}_1] - f_{3,2}[\boldsymbol{\eta}_2])$$
$$+ \tilde{\kappa}_i (f_{2,1}[\boldsymbol{\eta}_3] - f_{3,2}[\boldsymbol{\eta}_4] - f_{2,2}[\boldsymbol{\eta}_5] - f_{3,3}[\boldsymbol{\eta}_6])\}, \quad (47)$$

where form factors $\mathcal{F}_i \in \{\mathcal{V}, \mathcal{A}_1, \mathcal{T}_1, \mathcal{T}_2, \mathcal{A}_0, \mathcal{A}_{12}, \mathcal{T}_{23}\}$ with the replacement $f_V \to f_V^{\perp}$ for the first four $\mathcal{F}_i$ and $f_V \to f_V^{\parallel}$ for the last three $\mathcal{F}_i$, and the corresponding symmetry-breaking factors read as

$$\kappa_i \in \left\{1, -1, \frac{n\cdot q}{m_B}, -\frac{n\cdot q}{m_B}, -\frac{2m_V n\cdot q}{m_B n\cdot p}, \frac{2m_V n\cdot q}{m_B n\cdot p}, \frac{2m_V}{n\cdot p}\right\}, \quad (48)$$

$$\tilde{\kappa}_i \in \left\{1, 1, \frac{\bar{n}\cdot q}{m_B}, \frac{\bar{n}\cdot q}{m_B}, \frac{2m_V}{n\cdot p}, \frac{2m_V}{n\cdot p}, \frac{2m_V}{n\cdot p}\right\}, \quad (49)$$

and the density functions $\boldsymbol{\eta}_i$ are given as follows:

$$\boldsymbol{\eta}_1(\omega) = (\omega - 2\bar{\Lambda})\phi_B^+(\omega) + (m_{q'} \pm m_q)\phi_B^-(\omega),$$
$$\boldsymbol{\eta}_2(\omega_1, \omega_2, u) = 2[u\Phi_4(\omega_1, \omega_2) + \Psi_4(\omega_1, \omega_2)],$$
$$\boldsymbol{\eta}_3(\omega) = 0, \qquad \boldsymbol{\eta}_4(\omega_1, \omega_2, u) = 2\bar{u}\Psi_5(\omega_1, \omega_2),$$
$$\boldsymbol{\eta}_5(\omega) = \omega(2\bar{\Lambda} - \omega)\phi_B^-(\omega) + (m_q^2 - m_{q'}^2)\phi_B^-(\omega),$$
$$\boldsymbol{\eta}_6(\omega_1, \omega_2, u) = 2(\omega_1 + u\omega_2)\boldsymbol{\eta}_4(\omega_1, \omega_2, u), \quad (50)$$

where the + sign and − sign in $\boldsymbol{\eta}_1(\omega)$ are assigned to $\mathcal{F}_i \in \{\mathcal{V}, \mathcal{A}_1, \mathcal{T}_1, \mathcal{T}_2\}$ and $\mathcal{F}_i \in \{\mathcal{A}_0, \mathcal{A}_{12}, \mathcal{T}_{23}\}$, respectively.

C. Subleading heavy-quark effective current

We now proceed to consider the contributions of the power-suppressed terms in the heavy quark expansion to the $B \to K^*$ form factors. In HQET, the bottom quark can be replaced by the effective heavy quark field, and the heavy-to-light weak current is expanded up to NLP accuracy [47,54],

$$\bar{q}\Gamma_\mu b = \underbrace{\bar{q}\Gamma_\mu h_v}_{\mathrm{LP}} + \underbrace{\frac{1}{2m_b}\bar{q}\Gamma_\mu i\vec{\not{D}} h_v}_{\mathrm{NLP}} + \cdots, \quad (51)$$

where $\vec{\mathcal{D}} = \mathcal{D} - (v\cdot D)\not{v}$ and $\vec{\mathcal{D}} h_v(0) = [\mathcal{D} - (v\cdot D)\not{v}]h_v(0) = \mathcal{D} h_v(0)$ due to the HQET equations of motion. The ellipses denote the terms in powers of $\mathcal{O}(1/m_b^2)$, whose contributions to the correlation functions are beyond the scope of our current work. Substituting the heavy-to-light effective current in the correlation functions with the NLP term and taking advantage of the operator identities in Eq. (39) and the following equation,

$$\bar{q}(x)\Gamma[x,0]\overrightarrow{D_\rho} h_v(0) = \partial_\rho[\bar{q}(x)\Gamma[x,0]h_v(0)] + i\int_0^1 du\bar{u}\,\bar{q}(x)[x,ux]g_s G_{\lambda\rho}(ux)[ux,0]x^\lambda \Gamma h_v(0)$$
$$- \frac{\partial}{\partial x^\rho}\bar{q}(x)\Gamma[x,0]h_v(0), \quad (52)$$

the correlation functions can be directly presented in the following form:

$$\Pi_{j,\mathrm{NLP}}^{(a),\mathrm{HQE}}(p,q) = \int d^4x e^{ip\cdot x}\langle 0|T\{\bar{q}'(x)\Gamma_j q(x), \frac{1}{2m_b}\bar{q}(0)\Gamma_\mu^{(a)} i\vec{\not{D}} h_v\}|\bar{B}(p+q)\rangle$$
$$= \frac{-1}{2m_b}\int d^4x \int \frac{d^4k}{(2\pi)^4}\frac{e^{ik\cdot x}}{\bar{n}\cdot p - \bar{n}\cdot k + i\epsilon}\left\{\partial_\xi\left[\bar{q}(x)\Gamma_j \frac{\not{\bar{n}}}{2}\Gamma_\mu^{(a)}\gamma_\xi h_v(0)\right]\right.$$
$$\left. + i\int_0^1 du\bar{u}\,\bar{q}(x)x^\rho g_s G_{\rho\xi}(ux)\Gamma_j \frac{\not{\bar{n}}}{2}\Gamma_\mu^{(a)}\gamma^\xi h_v(0) - \frac{\partial}{\partial x_\xi}[\bar{q}(x)]\Gamma_j \frac{\not{\bar{n}}}{2}\Gamma_\mu^{(a)}\gamma_\xi h_v(0)\right\}, \quad (53)$$

where $a \in \{\mathrm{V}-\mathrm{A}, \mathrm{T}+\tilde{\mathrm{T}}\}$ denotes the different Dirac structures $\Gamma_\mu^{(a)} \in \{\gamma_\mu(1-\gamma_5), i\sigma_{\mu\nu}(1+\gamma_5)q^\nu\}$ and $\Gamma_j \in \{\frac{\not{n}}{2}, \frac{\not{\bar{n}}}{2}\gamma_\delta^{\perp}\}$ for $j = \parallel, \perp$, respectively. We can further derive the factorization formula by utilizing analogous techniques at tree level:

$$\Pi^{(a),\mathrm{HQE}}_{j,\mathrm{NLP}} = \Gamma^{(a)}_j \frac{\tilde{f}_B(\mu) m_B}{4 m_b} \left\{ \int_0^\infty d\omega \frac{1}{\bar{n}\cdot p - \omega} [(2\bar{\Lambda} - \omega)\phi_B^+(\omega) + (\bar{\Lambda} - \omega - m_{q'})\phi_B^-(\omega)] + \int_0^\infty d\omega_1 \int_0^\infty d\omega_2 \int_0^1 du \frac{2[\Phi_4(\omega_1,\omega_2) + \Psi_4(\omega_1,\omega_2)]}{(\bar{n}\cdot p - \omega_1 - u\omega_2)^2} \right\}, \tag{54}$$

with

$$\Gamma^{\mathrm{V-A}}_{\parallel,\perp} \in \{-\bar{n}_\mu, g^\perp_{\delta\mu} + i\epsilon^\perp_{\delta\mu}\},$$
$$\Gamma^{\mathrm{T+\tilde{T}}}_{\parallel,\perp} \in \left\{ n_\mu \frac{\bar{n}\cdot q}{2} - \bar{n}_\mu \frac{n\cdot q}{2}, \bar{n}\cdot q (g^\perp_{\delta\mu} + i\epsilon^\perp_{\delta\mu}) \right\}. \tag{55}$$

By matching the partonic representation with the hadronic dispersion relations given from Eqs. (15) to (18), we can derive the subleading-power heavy-quark effective current correction to the $B \to K^*$ form factors

$$f_V \exp\left[-\frac{m_V^2}{n\cdot p \omega_M}\right] \mathcal{F}^{\mathrm{HQE}}_{i,\mathrm{NLP}}(q^2) = \frac{\tilde{f}_B(\mu) m_B}{2(n\cdot p) m_b} c_i \{ f_{2,1}[\boldsymbol{\zeta}_1] + f_{3,2}[\boldsymbol{\zeta}_2] \}, \tag{56}$$

where the coefficient factors c_i are determined from the correlation functions at the hadronic level,

$$c_i \in \left\{ -1, -1, \frac{\bar{n}\cdot q}{m_B}, \frac{\bar{n}\cdot q}{m_B}, \frac{2m_V}{n\cdot p}, \frac{2m_V}{n\cdot p}, \frac{-2m_V}{n\cdot p} \right\}, \tag{57}$$

and the density functions $\boldsymbol{\zeta}_i$ can be derived from the correlation functions at the partonic level in Eq. (54):

$$\boldsymbol{\zeta}_1(\omega) = (2\bar{\Lambda} - \omega)\phi_B^+(\omega) + (\bar{\Lambda} - \omega - m_{q'})\phi_B^-(\omega),$$
$$\boldsymbol{\zeta}_2(\omega_1,\omega_2,u) = 2[\Phi_4(\omega_1,\omega_2) + \Psi_4(\omega_1,\omega_2)]. \tag{58}$$

Both the correction from the hard-collinear propagator and the correction from the subleading effective current to the $B \to K^*$ form factors show excellent agreement with the previous calculation for the $B \to D^*$ process reported in Ref. [38], upon substituting the charm quark mass with the strange quark mass.

D. Higher-twist four-particle contribution

We are now in the position to calculate the heavy-to-light B-meson decay form factors from the twist-five and twist-six four-particle LCDAs in the factorization approximation. The subleading-power correction to the $B \to K^*$ form factors can be factorized into a product of the lower-twist two-particle LCDAs and the quark condensate [54,55]. By evaluating the lowest-order Feynman diagrams shown in Fig. 3, we obtain the nonleading Fock-state correction to the correlation functions

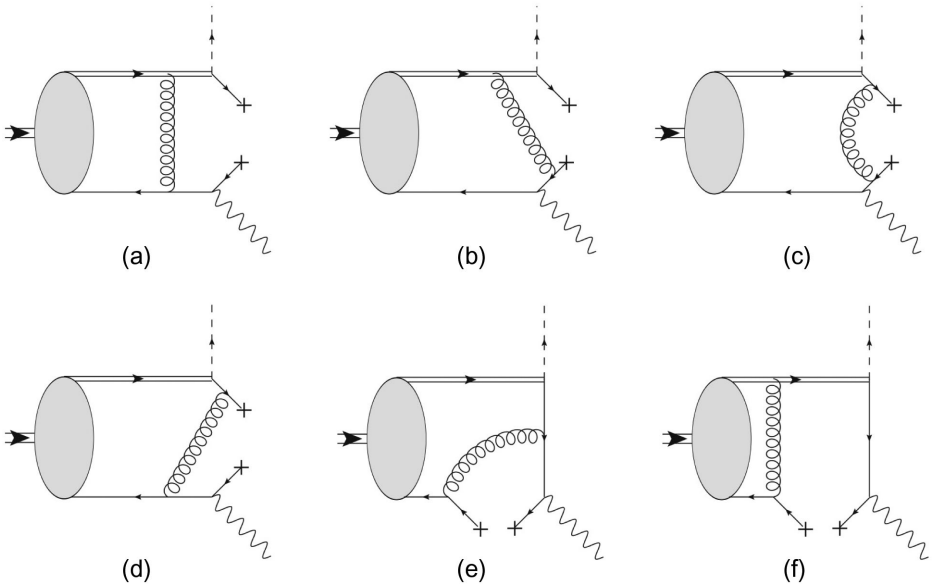

FIG. 3. Diagrammatic representations of twist-five and twist-six four-particle corrections to the vaccumm-to-bottom meson correlation functions. (a) and (f) describe the radiative correction between heavy quark and spectator quark; (b) describes the QCD correction to the weak vertex; (c) describes the self-energy correction to the quark propagator; (d) and (e) describe the QCD correction to the K^* vertex.

$$\Pi^{(a),4\mathrm{P}}_{j,\mathrm{NLP}} = \frac{g_s^2 C_F}{12}\frac{\tilde{f}_B(\mu) m_B}{n\cdot p}\left\{\Gamma_j^{(a)}\langle\bar{q}q\rangle\int_0^\infty d\omega \frac{\phi_B^+(\omega)}{\bar{n}\cdot p(\omega-\bar{n}\cdot p)^2} + \tilde{\Gamma}_j^{(a)}\langle\bar{q}'q'\rangle\int_0^\infty d\omega\frac{\phi_B^+(\omega)}{\omega^3}\left[\frac{2\omega}{\bar{n}\cdot p-\omega}-\frac{\omega^2}{\bar{n}\cdot p(\bar{n}\cdot p-\omega)}+2\ln\frac{\bar{n}\cdot p-\omega}{\bar{n}\cdot p}\right]\right\}, \tag{59}$$

with $\Gamma_\parallel^{(a)} = \tilde{\Gamma}_\parallel^{(a)} = \{\bar{n}_\mu, n_\mu\frac{\bar{n}\cdot q}{2} - \bar{n}_\mu\frac{n\cdot q}{2}\}$ and $\Gamma_\perp^{(a)} = 0, \tilde{\Gamma}_\perp^{(a)} = \{g_{\delta\mu}^\perp + i\epsilon_{\delta\mu}^\perp, -\bar{n}\cdot q(g_{\delta\mu}^\perp + i\epsilon_{\delta\mu}^\perp)\}$ for $a\in\{\mathrm{V-A}, \mathrm{T+\tilde{T}}\}$. $\Gamma_j^{(a)}$ and $\tilde{\Gamma}_j^{(a)}$ denote the contributions from diagram (d) and diagram (e) in Fig. 3, respectively. The terms $\langle\bar{q}q\rangle$ and $\langle\bar{q}'q'\rangle$ represent the vacuum condensate of the propagator quark q and the spectator quark q', respectively.

It is worth mentioning that diagram (e) in Fig. 3 is analyzed using the background field expansion of the quark propagator on the light cone [51],

$$\langle 0|T\{q(x),\bar{q}(0)\}|0\rangle \supset \frac{\Gamma(d/2-1)}{8\pi^{d/2}(-x^2)^{d/2-1}}\int_0^1 duu\bar{u}\not{x}g_s D_\lambda G^{\lambda\rho}(ux)x_\rho + \frac{\Gamma(d/2-2)}{16\pi^{d/2}(-x^2)^{d/2-2}}\int_0^1 du\left(u\bar{u}-\frac{1}{2}\right)g_s D_\lambda G^{\lambda\rho}(ux)\gamma_\rho, \tag{60}$$

where the classical equation of motion in QCD reads as

$$D^\lambda G^a_{\lambda\rho} = -g_s\sum_q \bar{q}\gamma_\rho T^a q. \tag{61}$$

After explicitly calculating diagrams (a), (b), and (c) in Fig. 3, the results indicate that, in comparison to the dominant contributions from diagrams (d) and (e), these three diagrams can only contribute to the higher power corrections. Moreover, diagram (f) is found to be insensitive to both the hard and hard-collinear QCD dynamics. Furthermore, diagram (d) is power suppressed relative to diagram (e) when the interpolating current corresponds to a transversely polarized K^*.

By applying the dispersion relation to the correlation functions at the partonic level and employing the standard sum rule approach, we can derive the subleading-power corrections from four-particle contributions to the $B\to K^*$ form factors

$$f_V\exp\left[-\frac{m_V^2}{n\cdot p\omega_M}\right]\mathcal{F}^{4\mathrm{P}}_{i,\mathrm{NLP}}(q^2) = \frac{2\pi\alpha_s C_F\tilde{f}_B(\mu)m_B}{3(n\cdot p)^2}c_i\langle\bar{q}'q'\rangle\left\{\int_0^{\omega_s}d\omega\phi^+_{\text{eff-I}}(\omega) + \int_{\omega_s}^\infty d\omega\phi^+_{\text{eff-II}}(\omega) - r_i\frac{\langle\bar{q}q\rangle}{\langle\bar{q}'q'\rangle}\left[e^{-\frac{\omega_s}{\omega_M}}\frac{\phi_B^+(\omega_s)}{\omega_s} - \int_{\omega_s}^\infty d\omega\frac{\phi_B^+(\omega)}{\omega^2} + \int_0^{\omega_s}d\omega\phi^+_{\text{eff-III}}(\omega)\right]\right\}, \tag{62}$$

where the coefficients

$$c_i\in\left\{1,1,\frac{\bar{n}\cdot q}{m_B},\frac{\bar{n}\cdot q}{m_B},\frac{2m_V}{n\cdot p},\frac{2m_V}{n\cdot p},\frac{2m_V}{n\cdot p}\right\},$$
$$r_i\in\{0,0,0,0,1,1,1\} \tag{63}$$

for $\mathcal{F}_i\in\{\mathcal{V},\mathcal{A}_1,\mathcal{T}_1,\mathcal{T}_2,\mathcal{A}_0,\mathcal{A}_{12},\mathcal{T}_{23}\}$ and the explicit expressions for the density functions ϕ_{eff} are given by

$$\phi^+_{\text{eff-I}}(\omega) = \left[1-2\frac{\omega_M}{\omega}+\left(1+2\frac{\omega_M}{\omega}\right)e^{-\frac{\omega}{\omega_M}}\right]\frac{\phi_B^+(\omega)}{\omega^2},$$
$$\phi^+_{\text{eff-II}}(\omega) = \left[1-2\frac{\omega_M}{\omega}+2\frac{\omega_M}{\omega}e^{-\frac{\omega_s}{\omega_M}}\right]\frac{\phi_B^+(\omega)}{\omega^2},$$
$$\phi^+_{\text{eff-III}}(\omega) = \left[\left(1+\frac{\omega}{\omega_M}\right)e^{-\frac{\omega}{\omega_M}}-1\right]\frac{\phi_B^+(\omega)}{\omega^2}. \tag{64}$$

Collecting the next-to-leading power (NLP) contributions estimated above, the total NLP correction to the $B\to K^*$ form factors in QCD can be expressed as

$$F^i_{BK^*,\mathrm{NLP}} = F^{i,\mathrm{HT}}_{BK^*,\mathrm{NLP}} + F^{i,\mathrm{QPE}}_{BK^*,\mathrm{NLP}} + F^{i,\mathrm{HQE}}_{BK^*,\mathrm{NLP}} + F^{i,4\mathrm{P}}_{BK^*,\mathrm{NLP}}, \tag{65}$$

where the index i labels seven different $B\to K^*$ form factors in QCD. Before proceeding to the numerical analysis, we first establish the power-counting rules for the form factors at LP and NLP, adopting the asymptotic behaviors of B-meson LCDAs [50]. According to the power-counting scheme $\omega_M\sim\omega_s\sim\mathcal{O}(\lambda^2)$ and $m_s\sim\mathcal{O}(\lambda)$, where the scaling parameter $\lambda=\Lambda_{\mathrm{QCD}}/m_b$, we derive the scaling behavior for the leading-power $B\to K^*$ form factors,

$$V^{\rm LP}_{BK^*} \sim A^{\rm LP}_{1,BK^*} \sim T^{\rm LP}_{1,BK^*} \sim T^{\rm LP}_{2,BK^*} \sim \mathcal{O}(\lambda^2),$$
$$A^{\rm LP}_{0,BK^*} \sim \mathcal{O}(\lambda^3), \qquad A_{12}{}^{\rm LP}_{BK^*} \sim T_{23}{}^{\rm LP}_{BK^*} \sim \mathcal{O}(\lambda^4), \tag{66}$$

where A_{12} and T_{23} denote combinations of the form factors corresponding to $\frac{m_B+m_V}{n\cdot p}A_1 - \frac{m_B-m_V}{m_B}A_2$ and $\frac{m_B}{n\cdot p}T_2 - T_3$, respectively. From the relations between seven QCD form factors and the four SCET effective form factors in Ref. [31], the scalings of the form factors V, A_1, T_1, T_2 are determined by the SCET effective form factor $\xi_\perp$, while A_0, A_{12}, T_{23} are determined by the SCET effective form factor $\xi_\parallel$. Evidently, $\xi_\parallel$ is suppressed by a factor of λ^2 compared to $\xi_\perp$. Because A_0 has an enhancement factor of $1/m_s$, it ultimately contributes the power of $\mathcal{O}(\lambda^3)$. Applying the same analytical method as for the leading power and considering the asymptotic behavior of two-particle and three-particle higher-twist B-meson LCDAs, we further determine the scalings of $B \to K^*$ form factors at NLP:

$$V^{\rm NLP}_{BK^*} \sim A^{\rm NLP}_{1,BK^*} \sim T^{\rm NLP}_{1,BK^*} \sim T^{\rm NLP}_{2,BK^*} \sim \mathcal{O}(\lambda^3),$$
$$A^{\rm NLP}_{0,BK^*} \sim \mathcal{O}(\lambda^4), \qquad A_{12}{}^{\rm NLP}_{BK^*} \sim T_{23}{}^{\rm NLP}_{BK^*} \sim \mathcal{O}(\lambda^5). \tag{67}$$

IV. NUMERICAL ANALYSIS

Summing up both the NLL correction and the newly derived NLP corrections, we obtain the improved $B \to K^*$ form factors with SCET sum rules in the large recoil region. In this section, we analyze phenomenological observables for the rare FCNC process $B \to K^*\nu_\ell\bar{\nu}_\ell$. We firstly list the relevant theoretical inputs in the factorization formula for the heavy-to-light form factors, including quark masses, decay constants, distribution amplitudes, sum rules parameters, electroweak parameters, and the inverse moments. We compare the form factors under two scenarios: selecting the inverse moment as either the recent lattice QCD simulation result $\lambda_B = 389(35)$ MeV or the conventional range $\lambda_B = 350(150)$ MeV. The theoretical precision of form factors could be improved if lattice QCD simulations systematically account for potential uncertainties [56]. After taking into account both the available lattice QCD results in the high-q^2 region and improved LCSR predictions in the low-q^2 region, we then perform a combined fit to determine the coefficients in the z-series expansion, thereby extending the $B \to K^*$ form factors to the entire kinematic region. Taking advantage of the newly updated LCSR predictions, we investigate the differential branching ratio and longitudinal K^* polarization fraction of $B \to K^*\nu_\ell\bar{\nu}_\ell$ decays. For the $B^+ \to K^{*+}\nu_\ell\bar{\nu}_\ell$ decay process, the additional long-distance effect induced by $B^+ \to \tau^+(\to K^{*+}\nu_\tau)\bar{\nu}_\tau$ at tree level is included with the narrow τ width approximation.

A. Theory inputs

In Table I, we summarize the necessary input parameters of the Standard Model and relevant hadronic parameters, along with the central values and uncertainties. In our numerical calculations, we employ the three-loop evolution of the strong coupling constant $\alpha_s(\mu)$ in the Modified Minimal Subtraction ($\overline{\rm MS}$) scheme by taking the interval $\alpha_s^{(5)}(m_Z)$ from [57] and adopting the perturbative matching scales $\mu_4 = 4.8$ GeV and $\mu_3 = 1.3$ GeV for crossing the $n_f = 4$ and $n_f = 3$ thresholds, respectively [58,59]. Additionally, the bottom quark mass $m_b(m_b)$ and strange quark mass $m_s(m_s)$ are given in the $\overline{\rm MS}$ scheme at the scale of their respective $\overline{\rm MS}$ masses. Using **RunDec** [60], we obtain the scale dependence of the strong coupling constant

TABLE I. Numerical values of the input parameters.

Parameter	Value	Ref.	Parameter	Value	Ref.
m_{B^0}	5279.66 MeV	[57]	$m_{K^{*0}}$	898.46 MeV	[57]
m_{B^+}	5279.34 MeV	[57]	$m_{K^{*+}}$	891.67 MeV	[57]
τ_{B^0}	1.517(4) ps	[57]	τ_{B^+}	1.638(4) ps	[57]
m_{τ^+}	1776.86 MeV	[57]	τ_{τ^+}	0.2903(5) ps	[57]
G_F	1.166379×10^{-5} GeV^{-2}	[57]	$\sin^2\theta_W$	0.23126(5)	[72]
$\lvert V_{tb}V_{ts}^*\rvert$	$(41.25 \pm 0.45) \times 10^{-3}$	[73]	$\alpha_{em}(m_Z)$	1/127.925	[57]
$\lvert V_{ub}\rvert$	$3.82(20) \times 10^{-3}$	[57]	$\lvert V_{us}\rvert$	0.2243(8)	[57]
$m_b(m_b)$	(4.203 ± 0.011) GeV	[57]	$m_s(m_s)$	(93.5 ± 0.8) MeV	[57]
f_B	(190.0 ± 1.3) MeV	[61]	μ_{h1}	$[m_b/2, 2m_b]$	
$f_{K^*}^{\parallel}$	(204 ± 7) MeV	[27]	μ_{h2}	$[m_b/2, 2m_b]$	
$f_{K^*}^{\perp}(1\ \text{Gev})$	(159 ± 6) MeV	[62]	μ	1.5 ± 0.5 GeV	
$\langle\bar{q}q\rangle(2\ \text{Gev})$	$-(286 \pm 23\ \text{MeV})^3$	[61]	ν	m_b	
$\langle\bar{s}s\rangle:\langle\bar{q}q\rangle$	(0.8 ± 0.1)	[74,75]	M^2	(1.7 ± 0.5) GeV^2	[71]
$s_0^{\parallel}$	(1.7 ± 0.1) GeV^2	[28,71]	$s_0^{\perp}$	(1.4 ± 0.1) GeV^2	[28,71]
λ_B	350 ± 150 MeV	[54]	$\{\hat{\sigma}_1, \hat{\sigma}_2\}$	$\{0.7, 6.0\}$	[54]
$(\lambda_E^2/\lambda_H^2)$	0.50 ± 0.10	[54]		$\{0.0, \pi^2/6\}$	
$(2\lambda_E^2 + \lambda_H^2)$	(0.25 ± 0.15) GeV^2	[54]		$\{-0.7, -6.0\}$	

$\alpha_s(\mu)$ and the quark masses $m_b(\mu)$ and $m_s(\mu)$. Moreover, we incorporate the results from four-flavor lattice QCD computations for the B-meson decay constant f_B [61]. The decay constant of the longitudinal K^* can be extracted from leptonic decays $V^0 \to e^+e^-$ and tau lepton decays $\tau^+ \to V^+\nu_\tau$, while the renormalization scale-dependent decay constant of the transverse K^* is taken from a lattice QCD simulation with $2+1$ flavors of domain wall quarks and the Iwasaki gauge action [62]. Two hard scales μ_{h1} and μ_{h2} are introduced in the hard functions and B-meson decay constants, respectively. The factorization scale μ is the same as the hard-collinear scale, and the renormalization scale for the QCD tensor current will be taken as $\nu = m_b$. The LCSR improved form factors for the B-meson semileptonic decay processes depend on the B-meson light cone distribution amplitudes (LCDAs) as universal nonperturbative input parameters. Therefore, we need to construct an acceptable phenomenological model for the leading- and higher-twist B-meson LCDAs that not only satisfies the classical equations of motion [50], but also exhibits the expected asymptotic behavior at sufficiently large scales. In this work, we adopt a newly proposed three-parameter model for all the relevant B-meson light cone distribution amplitudes in coordinate space [54], with the details provided in Appendix D. The three shape parameters α, β, and ω_0 in this model can be related to the inverse logarithmic moments λ_B and $\hat{\sigma}_{1,2}$ for the leading-twist B-meson distribution amplitude ϕ_B^+ with the equations

$$\begin{aligned}
\lambda_B(\mu) &= \frac{\alpha-1}{\beta-1}\omega_0,\\
\hat{\sigma}_1(\mu) &= \psi(\beta-1) - \psi(\alpha-1) + \ln\frac{\alpha-1}{\beta-1},\\
\hat{\sigma}_2(\mu) &= \hat{\sigma}_1^2(\mu) + \psi'(\alpha-1) - \psi'(\beta-1) + \frac{\pi^2}{6},
\end{aligned} \tag{68}$$

and the definitions of the inverse logarithmic moments λ_B and $\hat{\sigma}_{1,2}$ are

$$\begin{aligned}
\frac{1}{\lambda_B(\mu)} &= \int_0^\infty \frac{d\omega}{\omega}\phi_B^+(\omega,\mu),\\
\frac{\hat{\sigma}_n(\mu)}{\lambda_B(\mu)} &= \int_0^\infty \frac{d\omega}{\omega}\ln^n\frac{e^{-\gamma_E}\lambda_B(\mu)}{\omega}\phi_B^+(\omega,\mu).
\end{aligned} \tag{69}$$

The numerical values for the hadronic parameters λ_B, $\hat{\sigma}_{1,2}$, and $\lambda_{E,H}$ in Table I are all given at the reference scale $\mu_0 = 1$ GeV, and these parameters will be evolved to the factorization scale μ in the final results. Despite various strategies being employed to investigate the inverse moment λ_B [54,56,63–69], a QCD-based method for its precise determination remains elusive due to its definition via a nonlocal operator (see Refs. [56,70] for preliminary results from the lattice QCD perspectives). We adopt a conservative interval of $\lambda_B = (350 \pm 150)$ MeV in this work and compare the resulting form factors with those derived from $\lambda_B = 389(35)$ MeV, as suggested by the recent lattice QCD result [56,70]. For the inverse logarithmic moments $\hat{\sigma}_{1,2}$, we prefer the choice $\{\hat{\sigma}_1, \hat{\sigma}_2\} = \{0, \pi^2/6\}$ with the intervals

$$-0.7 < \hat{\sigma}_1 < 0.7, \qquad -6.0 < \hat{\sigma}_2 < 6.0. \tag{70}$$

Following the standard procedure outlined in Refs. [28,31,71], the two intrinsic parameters ω_M and ω_s introduced by the light cone sum rules can be determined by effectively constraining the smallness of the continuum contributions in the dispersion integrals and the stability of the obtained sum rule results against the variation of ω_M. The parameters $s_0^\perp$ and $s_0^\parallel$ correspond to the interpolating currents $\bar{q}'\not{n}\gamma_\perp q$ and $\bar{q}'\not{n}q$, respectively, leading to the following intervals:

$$\begin{aligned}
s_0^\perp &= n\cdot p\omega_s^\perp = (1.4 \pm 0.1)\text{GeV}^2,\\
s_0^\parallel &= n\cdot p\omega_s^\parallel = (1.7 \pm 0.1)\text{GeV}^2,\\
M^2 &= n\cdot p\omega_M = (1.7 \pm 0.5)\text{GeV}^2.
\end{aligned} \tag{71}$$

B. Numerical predictions for the $B \to K^*$ form factors

Making use of the numerical inputs from Table I and the B-meson light cone distribution amplitudes described by the three-parameter model in Appendix D, we obtain the $B \to K^*$ form factors in the large recoil region. In Table II, we present the numerical results of $B \to K^*$ form factors based on LCSR with heavy-meson distribution amplitudes at $q^2 = 0$. The central values of our improved form factors are consistent within a $1 \sim 2\sigma$ deviation with the results obtained from sum rules based on K^* distribution amplitudes [27]. To examine the numerical features of the LCSR parameters to form factors, we first present the dependence of the form factors on the Borel mass M^2 in Fig. 4. The left panel in Fig. 4 shows the variation of form

TABLE II. The $B \to K^*$ form factors at $q^2 = 0$ given by our work (second row) and by sum rules with light-meson distribution amplitudes (third row).

$\mathcal{F}_i^{B\to K^*}$	$\mathcal{V}$	$\mathcal{A}_0$	$\mathcal{A}_1$	$\mathcal{T}_1$	$\mathcal{T}_2$	$\mathcal{A}_{12}$	$\mathcal{T}_{23}$
This work	0.20(14)	0.066(38)	0.19(13)	0.24(16)	0.19(13)	0.066(38)	0.094(44)
Ref. [27]	0.29(3)	0.118(16)	0.306(33)	0.282(31)	0.274(31)	0.113(15)	0.095(13)

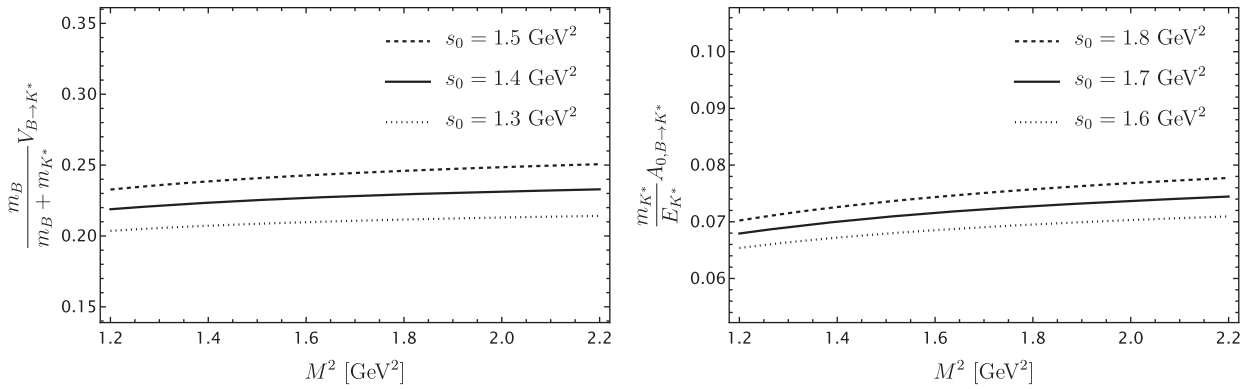

FIG. 4. Dependence of the form factors $\mathcal{V}_{B\to K^*}$ and $\mathcal{A}_{0,B\to K^*}$ on the Borel parameter M^2.

factor $\mathcal{V}$ when the Borel mass M^2 changes in the range of 1.2 GeV^2 to 2.2 GeV^2, with the effective threshold $s_0^{\perp}$ fixed at 1.3 GeV^2, 1.4 GeV^2, and 1.5 GeV^2. The right panel in Fig. 4 illustrates the effect on the form factor $\mathcal{A}_0$ for the same Borel mass range, with the effective threshold set at 1.6 GeV^2, 1.7 GeV^2, and 1.8 GeV^2, respectively. We find that LCSR form factors exhibit a mild dependence on the intrinsic parameters M^2 and $s_0^{\parallel,\perp}$, with each introducing 10% systematic uncertainties to the form factors, which is consistent with our previous work [31] and other sum rule analyses [36,37].

We now proceed to explore the contributions of the subleading-power corrections from different sources to the $B \to K^*$ form factors, with the form factors $\mathcal{V}$ and $\mathcal{A}_0$ as illustrative examples. In Fig. 5, we present the contributions of four different sources of the subleading-power corrections as well as the total power correction in the kinematic region of $0 \le q^2 \le 6$ GeV^2. These subleading-power corrections include the "HT " contribution from the two-particle and three-particle higher-twist B-meson distribution amplitudes, the "QPE " contribution from the expansion of hard-collinear quark propagator in the small parameter $\Lambda_{\rm QCD}/m_b$, the "HQE " contribution from the power-suppressed effective weak transition current $\bar{q}\Gamma[i\not{D}_\perp/(2m_b)]h_v$, and the "4P " contribution from twist-5 and twist-6 four-particle B-meson LCDAs within the factorization approach. We can find that the NLP contribution from twist-5 and twist-6 four-particle B-meson LCDAs is minimal for the $B \to K^*$ form factors, and this contribution accounts for only $3\% - 7\%$ of the total NLP contribution to the form factors $\mathcal{V}$ and $\mathcal{A}_0$, respectively. In contrast, it is evident that the higher-twist B-meson LCDAs provide the largest contributions to the NLP $B \to K^*$ form factors, which numerically account for $50\% - 60\%$ of the total NLP corrections in analogy to the previous discussions [29,36,37,76].

We now explore the contribution of the NLL resummation improved leading-power $B \to K^*$ form factors and the newly derived subleading-power corrections to the $B \to K^*$ form factors at tree level. In order to understand the impact of one-loop and subleading-power corrections, we show the numerical results explicitly for the resummation improved contribution at the one-loop level and NLP corrections at the tree level to the $B \to K^*$ form factors in the region of $0 \le q^2 \le 6$ GeV^2 in Fig. 6. For instance, the resummation improved NLL correction reduces the form factors $\mathcal{V}$ and $\mathcal{A}_0$ by 30% compared to the results at leading-logarithm accuracy. In addition, the newly determined NLP

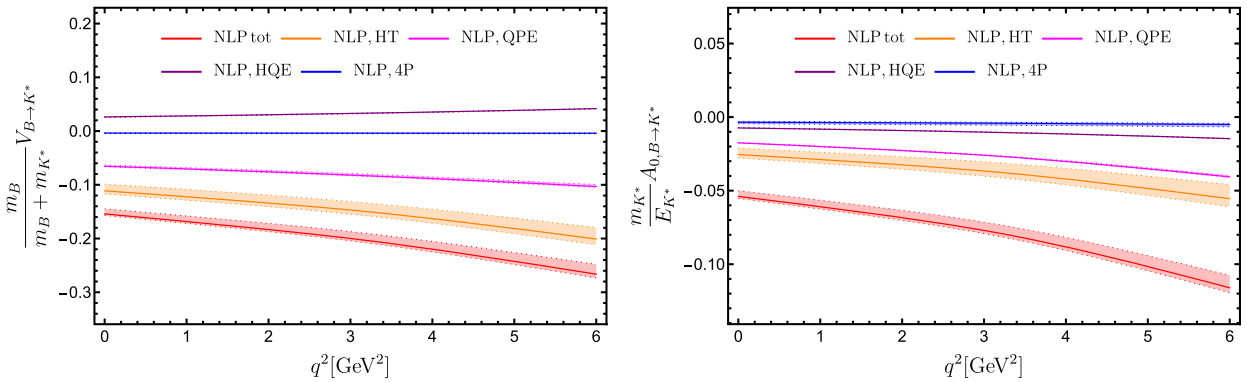

FIG. 5. Subleading-power corrections to the $B \to K^*$ form factors $\mathcal{V}_{B\to K^*}$ (left panel) and $\mathcal{A}_{0,B\to K^*}$ (right panel) in the kinematic region of $0 \le q^2 \le 6$ GeV^2. The shaded bands represent the uncertainties from the variation of factorization scale μ.

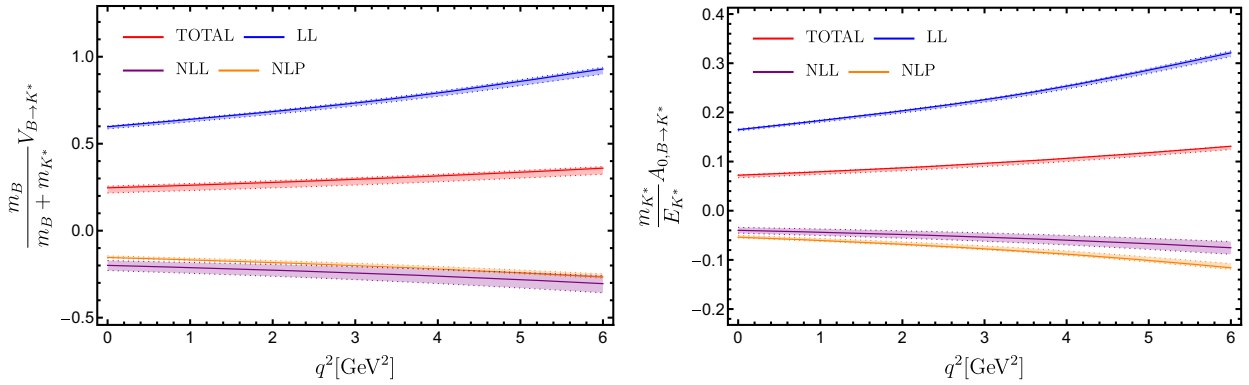

FIG. 6. Comparison of the LL resummation improved tree-level contribution (LL), NLL resummation improved one-loop correction (NLL), subleading-power correction at tree level (NLP), and total result (TOTAL) to the $B \to K^*$ form factors $\mathcal{V}_{B\to K^*}$ (left panel) and $\mathcal{A}_{0,B\to K^*}$ (right panel) in the kinematic region of $0 \le q^2 \le 6$ GeV^2. The shaded bands represent the uncertainties from the variation of factorization scale μ.

corrections lead to an approximate 30% reduction to the form factors $\mathcal{V}$ and $\mathcal{A}_0$, respectively. After including both NLP and NLL corrections, we find that the total results for the form factors $\mathcal{V}$ and $\mathcal{A}_0$ exhibit a 60% reduction relative to the corresponding LL resummation improved tree-level predictions.

In addition, we investigate the dependence of both the NLL resummation improved one-loop correction and the newly derived NLP corrections on the inverse moment λ_B at $q^2 = 0$. We take $\{\hat{\sigma}_1, \hat{\sigma}_2\} = \{0, \pi^2/6\}$ as the central values and display the corresponding numerical results in Fig. 7. For instance, we observe that the form factors $\mathcal{V}_{B\to K^*}$ and $\mathcal{A}_{0,B\to K^*}$ exhibit a pronounced decrease with increasing λ_B. By adopting $\lambda_B = 389(35)$ MeV as input from the lattice QCD in Ref. [70], we find that both the central values and uncertainties of the form factors are reduced by approximately 20% compared to those obtained with $\lambda_B = 350(150)$ MeV. Notably, the light cone sum rules based on light-meson LCDA suggest $\lambda_B \approx 300$ MeV, when fitting λ_B by using the form factor values from Ref. [27]. This discrepancy between $\lambda_B \approx 300$ MeV and the $\lambda_B = 389$ MeV derived by lattice QCD may stem from unaccounted power corrections in current lattice QCD simulations, which could potentially introduce additional systematic uncertainties.

Since LCSR predictions are valid only in the large recoil region, it is necessary to extrapolate the LCSR results for the $B \to K^*$ form factors to the entire kinematic region by employing the BCL z-series expansion [39–41,77,78], which is based on the positivity and analyticity of the transition form factors. For this purpose, we apply the conformal transformation

$$z(q^2, t_0) = \frac{\sqrt{t_+ - q^2} - \sqrt{t_+ - t_0}}{\sqrt{t_+ - q^2} + \sqrt{t_+ - t_0}} \tag{72}$$

with the threshold parameter $t_+ \equiv (m_B + m_{K^*})^2$ for the exclusive $B \to K^*$ form factors, which allows us to map the complex cut q^2 plane onto the unit disk $|z(q^2, t_0)| \le 1$.

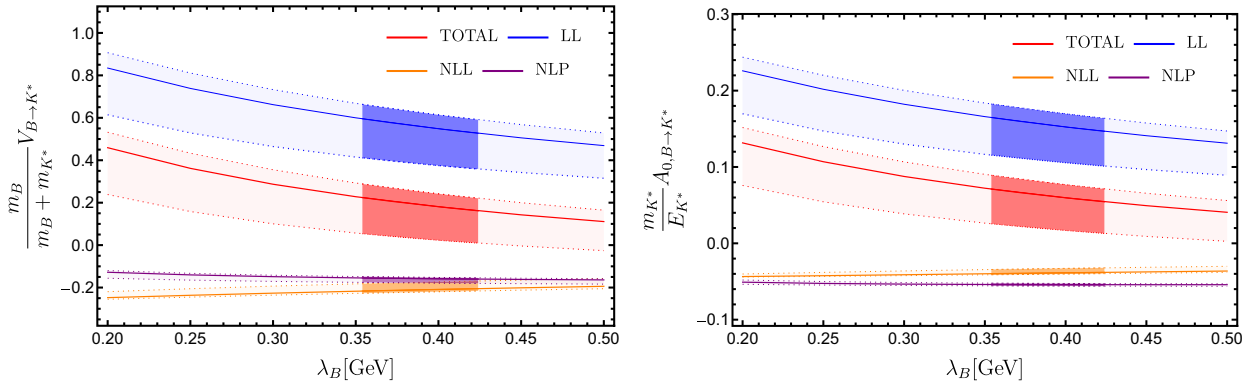

FIG. 7. Comparison of LL resummation improved tree-level contribution (LL), NLL resummation improved one-loop correction (NLL), subleading-power correction at tree level (NLP), and total result (TOTAL) of the $B \to K^*$ form factors $\mathcal{V}_{B\to K^*}$ (left panel) and $\mathcal{A}_{0,B\to K^*}$ (right panel) with the variation of 0.2 GeV $\le \lambda_B \le$ 0.5 GeV. The areas with deeper color correspond to $\lambda_B = 0.389(35)$ GeV given in Ref. [70]. The upper (lower) bound represents $\{\hat{\sigma}_1, \hat{\sigma}_2\} = \{-0.7, -6.0\}$ ($\{\hat{\sigma}_1, \hat{\sigma}_2\} = \{0.7, 6.0\}$).

Additionally, the free parameter $t_0 < t_+$ corresponds to the value of q^2 that is mapped onto the origin in the z plane. To minimize the z interval, we set

$$t_0 = t_+ - \sqrt{t_+(t_+ - t_-)}, \qquad t_- = (m_B - m_{K^*})^2. \tag{73}$$

Taking into account the asymptotic behavior of the form factor near the threshold of the corresponding excited states, we can further parametrize the $B \to K^*$ form factors with the z-series expansion as follows:

$$\mathcal{F}^i_{B\to K^*}(q^2) = \frac{1}{1 - q^2/m^2_{i,\text{pole}}} \sum_{k=0}^{N-1} b^i_k [z(q^2, t_0) - z(0, t_0)]^k, \tag{74}$$

where $m^2_{i,\text{pole}}$ denotes the masses of the corresponding resonances below the particle-pair production threshold $(m_B + m_{K^*})$ with distinct quantum numbers. For convenience, we have summarized the masses of the resonances relevant to our parametrization in Table III as given in Ref. [27]. We will truncate the z-series expansion at $N = 3$ in the subsequent fitting process, since the contribution beyond quadratic terms is negligible due to $|z(q^2)|_{\max} < 0.1$.

We are now in the position to determine the z-series coefficients $b^i_{0,1,2}$ of the $B \to K^*$ form factors $\mathcal{F}^i(q^2)$ by performing the correlated minimum-χ^2 fit of the updated LCSR predictions in the large recoil region, in combination with the available lattice QCD data in the small recoil region [13,14]. The ingredients of the minimum-χ^2 fit can be summarized as follows:

(1) In the low q^2 region, we generate the improved LCSR form factors with uncertainties at three distinct kinematic points $q^2 = \{-4, 0, 4\}$ GeV^2. In order to obtain the pseudodata samples, we vary the theoretical input parameters randomly within the error ranges and generate an ensemble of $N = 300$ parameter sets that follow uncorrelated priors, which are either uniform or Gaussian distributed [38].

(2) We multiply each form factor $\mathcal{F}^i_{\text{LCSR}}(q^2)$ by an enhancement factor $W_{K^*} = 1.09(1)$ to account for the finite K^* width effect in $B \to K^*$ transition, as discussed in Ref. [34]. In the lattice QCD simulation, K^* is a stable particle [13,14].

(3) In the high q^2 region, we reproduce the central values and correlation matrix of the lattice QCD results of the $B \to K^*$ form factors at three different points, $q^2 = \{12, 14, 16\}$ GeV^2, as well as physical-mass bottom quark and $2 + 1$ flavors of sea quarks. To ensure the positive definiteness of the correlation matrix from the lattice QCD results, we modify the original matrix by adding an additional diagonal matrix of order $\mathcal{O}(10^{-6})$, namely $C_{\text{latt}} = C_{\text{latt,original}} + 10^{-6}\text{I}$.

(4) Taking into account the kinematic constraints,

$$\frac{m_B + m_V}{2m_V} A_1(0) - \frac{m_B - m_V}{2m_V} A_2(0) = A_0(0), \qquad T_1(0) = T_2(0), \tag{75}$$

we can derive the following exact relations between the expansion coefficients,

$$\frac{m_V^2}{m_B^2 + m_V^2} b_0^{\mathcal{A}_1} - \frac{2m_B^2 + m_V^2}{m_B^2 + m_V^2} b_0^{\mathcal{A}_{12}} = b_0^{\mathcal{A}_0}, \qquad \frac{m_B^2}{m_B^2 + m_V^2} b_0^{\mathcal{T}_1} = b_0^{\mathcal{T}_2}. \tag{76}$$

(5) We then construct

$$\begin{aligned}\chi^2 = &\sum_{ij} [\mathcal{F}^i_{\text{LCSR}}(q^2) - \mathcal{F}^i_{\text{fit}}(q^2; b^i_k)](C^{-1}_{\text{LCSR}})_{ij} \\ &\times [\mathcal{F}^j_{\text{LCSR}}(q^2) - \mathcal{F}^j_{\text{fit}}(q^2; b^j_k)] \\ &+ \sum_{ij} [\mathcal{F}^i_{\text{latt}}(q^2) - \mathcal{F}^i_{\text{fit}}(q^2; b^i_k)](C^{-1}_{\text{latt}})_{ij} \\ &\times [\mathcal{F}^j_{\text{latt}}(q^2) - \mathcal{F}^j_{\text{fit}}(q^2; b^j_k)],\end{aligned} \tag{77}$$

where $\mathcal{F}^i$ denote the central values of the form factors and C_{ij} is the corresponding covariance matrix. We then extract the central values and the covariance of the coefficients b^i_k by minimizing the χ^2 function, yielding $\chi^2_{\min}/\text{d.o.f} = 40.1/23$. Our inputs as well as the fit results for the z-series coefficients, including the central values, uncertainties and all correlations, are presented in the Supplemental Material [79].

TABLE III. Summary of the resonance masses with distinct quantum numbers appearing in the z-series expansion of the $B \to K^*$ form factors in Eq. (74).

$\mathcal{F}^i_{B\to K^*}(q^2)$	J^P	$m_{i,pole}$ [GeV]
$\mathcal{V}(q^2)$, $\mathcal{T}_1(q^2)$	1^-	5.415
$\mathcal{A}_0(q^2)$	0^-	5.366
$\mathcal{A}_1(q^2)$, $\mathcal{A}_{12}(q^2)$, $\mathcal{T}_2(q^2)$, $\mathcal{T}_{23}(q^2)$	1^+	5.829

To further clarify the momentum-transfer dependence of the updated LCSR predictions and lattice QCD results, we present the combined fit results for the seven $B \to K^*$ form factors across the entire kinematic region in Fig. 8. BCL parametrization incorporates both our updated LCSR data (pink points) and lattice QCD data (blue points). For reference, lattice QCD predictions from prior studies are shown as a blue dot-dashed line. The inclusion of newly derived LCSR data in the low q^2 region substantially enhances the accuracy of theoretical predictions for the $B \to K^*$ form factors throughout the kinematic region, as

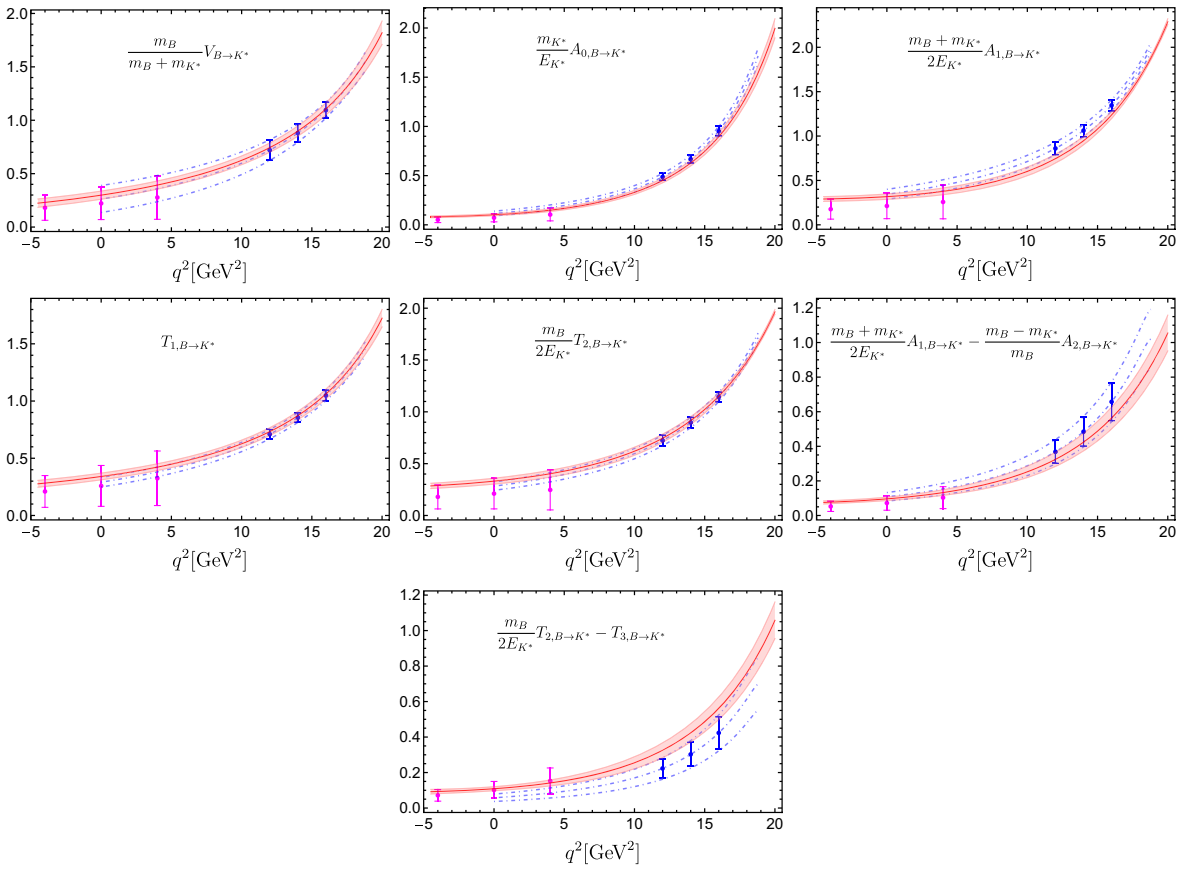

FIG. 8. Theoretical predictions of the $B \to K^*$ decay form factors (red band) obtained from the combined fit of updated LCSR (pink points) and lattice QCD (blue points) in the entire kinematical region. The "lattice QCD only" predictions for these form factors are indicated by the blue dot-dashed line for a comparison.

demonstrated by the combined fit with lattice QCD simulations.

C. Phenomenological analysis of the $B \to K^* \nu_\ell \bar{\nu}_\ell$ observables

The $B \to K^* \nu_\ell \bar{\nu}_\ell$ decays induced by the $b \to s$ FCNC represent one of the theoretically cleanest decay channels in heavy flavor physics. We now begin to explore the phenomenological implications of the newly determined $B \to K^*$ form factors for the electroweak penguin $B \to K^* \nu_\ell \bar{\nu}_\ell$ decays. Thanks to the high luminosity of the Belle II experiment, the exclusive rare $B \to K^* \nu_\ell \bar{\nu}_\ell$ decays are expected to be observed with 10 ab^{-1} of the data [80,81], and the previous experimental measurements by *BABAR* [82] and Belle [83,84] are also presented here. Notably, the precision of the total branching fraction measurement for $B \to K^* \nu_\ell \bar{\nu}_\ell$ with 50 ab^{-1} integrated luminosity is expected to reach approximately 10%, rendering the experimental sensitivity comparable to the current theoretical uncertainty in Standard Model predictions. Additionally, the longitudinal K^* polarization fraction, which is highly sensitive to right-handed currents [80], is projected to be measured with an absolute uncertainty of 0.1, providing critical insights into potential beyond-Standard Model contributions.

We are therefore well motivated to further investigate the phenomenological aspects of the $B \to K^* \nu_\ell \bar{\nu}_\ell$ process, both to gain a deeper understanding of the strong interaction dynamics of the $B \to K^*$ form factors and to explore the potential role of exotic particles X in the context of dark matter, utilizing the form factors derived in this work. It is straightforward to derive the differential decay width formula [10,85],

$$\frac{d\Gamma(B \to K^* \nu_\ell \bar{\nu}_\ell)}{dq^2} = \frac{G_F^2 \alpha_{em}^2}{256\pi^5} \frac{\lambda^{3/2}(m_B^2, m_{K^*}^2, q^2)}{m_B^3 \sin^4\theta_W} |\lambda_t|^2 \times \left[X_t\left(\frac{m_t^2}{m_W^2}, \frac{m_H^2}{m_t^2}, \sin\theta_W, \mu\right)\right]^2 \times [H_V(q^2) + H_{A_1}(q^2) + H_{A_{12}}(q^2)], \tag{78}$$

where $\lambda(x, y, z) = x^2 + y^2 + z^2 - 2xy - 2xz - 2yz$ is the Källen function. The Cabibbo-Kobayashi-Maskawa (CKM)

matrix elements $\lambda_t = |V_{tb}V_{ts}^*|$ can be determined by the **UT** *fit* Collaboration [73] and the input parameters appearing in the differential decay width are collected in Table I. The short-distance Wilson coefficient X_t can be expanded perturbatively in terms of the Standard Model coupling constants

$$X_t = X_t^{(0)} + \frac{\alpha_s}{4\pi} X_t^{\mathrm{QCD}(1)} + \frac{\alpha_{em}}{4\pi} X_t^{\mathrm{EW}(1)} + \cdots, \quad (79)$$

where the leading-order contribution $X_t^{(0)}$ [86], the next-to-leading-order (NLO) QCD correction $X_t^{\mathrm{QCD}(1)}$ [87–89], and the two-loop electroweak correction $X_t^{\mathrm{EW}(1)}$ [72] are already known analytically. We adopt $X_t = 1.469$ in our work. The three invariant functions H_i can be further expressed by the $B \to K^*$ form factors as

$$\begin{aligned} H_V(q^2) &= \frac{2q^2}{(m_B + m_{K^*})^2}[V(q^2)]^2, \\ H_{A_1}(q^2) &= \frac{2q^2(m_B + m_{K^*})^2}{\lambda(m_B^2, m_{K^*}^2, q^2)}[A_1(q^2)]^2, \\ H_{A_{12}}(q^2) &= \frac{64 m_B^2 m_{K^*}^2}{\lambda(m_B^2, m_{K^*}^2, q^2)}[A_{12}(q^2)]^2, \end{aligned} \quad (80)$$

with the helicity form factors A_{12} [13]

$$A_{12}(q^2) = \frac{(m_B + m_{K^*})^2(m_B^2 - m_{K^*}^2 - q^2)A_1(q^2) - \lambda(m_B^2, m_{K^*}^2, q^2)A_2(q^2)}{16 m_B m_{K^*}^2 (m_B + m_{K^*})}. \quad (81)$$

To probe new physics effects beyond the SM, λ_t is typically determined through CKM unitarity. However, inconsistencies persist in the extracted values of the CKM matrix element V_{cb} across different processes. For future studies, we present the CKM-independent branching ratio $|\lambda_t|^{-2}\mathcal{BR}(B^0 \to K^{*0}\nu_\ell\bar{\nu}_\ell)$ estimated with various strategies in Table IV. The branching ratios derived from updated $B \to K^*$ form factors agree within 2.5σ with the results obtained from sum rules based on K^* distribution amplitudes [27]. Additionally, in Fig. 9, we display our theoretical prediction for the CKM-independent differential branching fraction of $B^0 \to K^{*0}\nu_\ell\bar{\nu}_\ell$ and show the result from lattice QCD calculations for comparison. It is evident that the combined fit result exhibits significantly smaller uncertainty than lattice QCD predictions across the entire momentum region. Finally, our numerical results for the differential branching ratio of $B \to K^*\nu_\ell\bar{\nu}_\ell$ are summarized in Table V, where we have adopted $\lambda_t = 41.25 \times 10^{-3}$. The total uncertainty is dominated by the uncertainties in the hadronic form factors.

There is an additional long-distance (LD) contribution to the counterpart channel $B^+ \to K^{*+}\nu_\ell\bar{\nu}_\ell$ involving a charged B meson due to the double-charged current interaction $B^+ \to \tau^+(\to K^{*+}\nu_\tau)\bar{\nu}_\tau$, as originally discussed in Ref. [90]. In the narrow τ-lepton width limit, we express the tree-level LD contribution to the differential decay rate

$$\begin{aligned} &\frac{d\Gamma(B^+ \to K^{*+}\nu_\ell\bar{\nu}_\ell)}{dq^2}\Big|_{\mathrm{LD}} \\ &= \frac{G_F^4 |V_{ub}V_{us}^*|^2}{64\pi^2 m_B^3} |f_B f_{K^*}|^2 \frac{m_\tau^3}{\Gamma_\tau} \\ &\quad \times [(m_B^2 - m_\tau^2)(m_\tau^2 - m_{K^*}^2) - (m_\tau^2 - 2m_{K^*}^2)q^2]. \end{aligned} \quad (82)$$

This long-distance effect arising from weak annihilation mediated by the on shell τ lepton accounts for approximately 10% of the electroweak penguin amplitude, which is numerically significant for the charged channel $B^+ \to K^{*+}\nu_\ell\bar{\nu}_\ell$. Moreover, the interference effect between the tree and penguin amplitudes turns out to be negligible numerically due to the extremely small width of the τ lepton [90].

TABLE IV. The CKM-independent branching ratio of the $B^0 \to K^{*0}\nu_\ell\bar{\nu}_\ell$ process from updated form factors (left), lattice QCD form factors (middle) and LCSRs with K^*-meson LCDAs (right).

$10^{-3} \times (\lambda_t)^{-2}\mathcal{BR}$	This work	Ref. [13,14]	Ref. [27]
$B^0 \to K^{*0}\nu_\ell\bar{\nu}_\ell$	4.76(56)	5.86(93)	5.85(58)

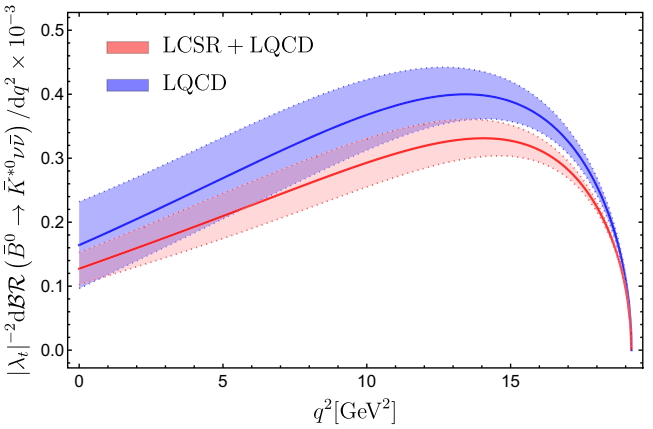

FIG. 9. Theory predictions for the CKM-independent differential branching fraction of $B^0 \to K^{*0}\nu_\ell\bar{\nu}_\ell$ by applying the form factors determined from the combined fits (pink band) and from the lattice simulations (blue band) [13,14].

TABLE V. Theory predictions for the integrated differential observables $\Delta\mathcal{BR}(q_1^2, q_2^2)$, and $\Delta F_L(q_1^2, q_2^2)$ obtained from the exclusive $B \to K^*$ form factors and additional long-distance contribution.

$[q_1^2, q_2^2]$(in GeV^2)	$10^6 \times \Delta\mathcal{BR}^{B^0\to K^{*0}\nu_\ell\bar{\nu}_\ell}(q_1^2, q_2^2)$	$10^6 \times \Delta\mathcal{BR}^{B^+\to K^{*+}\nu_\ell\bar{\nu}_\ell}(q_1^2, q_2^2)$	$\Delta F_L(q_1^2, q_2^2)$
[0.0, 1.0]	0.23(5)	0.33(5)	0.93(2)
[1.0, 2.5]	0.40(7)	0.55(8)	0.79(4)
[2.5, 4.0]	0.46(8)	0.61(9)	0.67(5)
[4.0, 6.0]	0.71(12)	0.91(13)	0.57(5)
[6.0, 8.0]	0.83(13)	1.03(14)	0.48(5)
[8.0, 12.0]	1.99(26)	2.39(28)	0.40(4)
[12.0, 16.0]	2.22(20)	2.61(22)	0.33(2)
$[16.0, (m_B - m_{K^*})^2]$	1.26(6)	1.53(7)	0.31(1)
$[0.0, (m_B - m_{K^*})^2]$	8.09(96)	9.95(1.05)	0.44(4)

We then proceed to define the differential longitudinal K^* polarization fraction F_L of the electroweak penguin decays $B \to K^*\nu_\ell\bar{\nu}_\ell$,

$$F_L(q^2) = \frac{H_{A_{12}}(q^2)}{H_V(q^2) + H_{A_1}(q^2) + H_{A_{12}}(q^2)}. \quad (83)$$

In addition, we introduce two q^2-binned observables for comparison with future high-luminosity Belle II data,

$$\Delta\mathcal{BR}(q_1^2, q_2^2) = \tau_B \int_{q_1^2}^{q_2^2} dq^2 \frac{d\Gamma(B \to K^*\nu_\ell\bar{\nu}_\ell)}{dq^2}, \quad (84)$$

$$\Delta F_L(q_1^2, q_2^2) = \frac{\int_{q_1^2}^{q_2^2} dq^2 \lambda^{3/2}(m_B^2, m_{K^*}^2, q^2) H_{A_{12}}(q^2)}{\int_{q_1^2}^{q_2^2} dq^2 \lambda^{3/2}(m_B^2, m_{K^*}^2, q^2)[H_V(q^2) + H_{A_1}(q^2) + H_{A_{12}}(q^2)]}.$$

Our predictions for these observables, with the choice of q^2 intervals following [80], are summarized in Table V. The theoretical uncertainties of the q^2-binned longitudinal K^* polarization fractions, ΔF_L, are significantly smaller than those of the branching ratio predictions, $\Delta\mathcal{BR}$, due to the reduced sensitivity of the form-factor ratios to the precise shapes of the B-meson distribution amplitudes.

V. SUMMARY

In this work, we have comprehensively investigated subleading-power corrections to the $B \to K^*$ form factors up to twist six within the framework of light cone sum rules (LCSR) with B-meson LCDAs. The corrections arise from two-particle and three-particle B-meson higher-twist light cone distribution amplitudes, power-suppressed terms in the expansion of the strange quark propagator, the subleading-power effective current $\bar{q}\Gamma[i\not{D}_\perp/(2m_b)]h_v$ in HQET, and the four-particle twist-five and twist-six B-meson LCDAs in the factorization approximation. Incorporating the leading-power contribution at NLL accuracy from Ref. [31] with our newly derived NLP contributions, we ultimately obtain updated predictions for the $B \to K^*$ form factors with SCET sum rules in the large recoil region. It is shown that power corrections account for approximately a 30% correction to the tree-level result, which is comparable to the NLL contribution. Moreover, we reach a similar conclusion that the dominant source of power corrections arises from the two-particle higher-twist B-meson LCDAs as in Ref. [29], while the impact of the four-particle corrections is numerically insignificant.

We employ a three-parameter model to describe the B-meson LCDAs and adopt the conventional inverse moment $\lambda_B = 350(150)$ MeV. In addition, we estimate the $B \to K^*$ form factors by adopting the inverse moment $\lambda_B = 389(35)$ MeV from recent lattice QCD calculations for comparison. The dominant uncertainties in the form factors originate from the inverse moments λ_B and $\{\sigma_1, \sigma_2\}$. In the future, lattice QCD studies may reduce the uncertainties of the inverse moments by systematically investigating subleading-power contributions via this first principle approach. By adopting the BCL parametrization and performing a combined fit of the newly derived LCSR predictions in the low q^2 region and the lattice QCD results in the high q^2 region, we extrapolate the $B \to K^*$ form factors to the entire momentum region. We find that the $B \to K^*$ form factors derived from the combined fits exhibit smaller uncertainties than those obtained solely using lattice data points. Furthermore, the combined fits to the LCSR and lattice QCD inputs for the $B \to K^*$ form factors not only provide predictions for the form factors that are applicable across the entire kinematic range, but also confirm the consistency of the two complementary methods by ensuring their agreement at intermediate q^2 values. Having at our disposal the $B \to K^*$ form factors in the entire momentum region, we proceed to predict the differential decay widths for $B \to K^*\nu_\ell\bar{\nu}_\ell$ processes, including long-distance effects in the charged $B \to K^*\nu_\ell\bar{\nu}_\ell$ decay. We present the CKM-independent differential branching ratio of $B^0 \to K^{*0}\nu_\ell\bar{\nu}_\ell$ obtained from the combined fits, alongside the lattice simulation result for comparison. The results

with different fit data inputs are consistent with each other, and the combined fits to the differential branching ratio of $B^0 \to K^{*0}\nu_\ell\bar{\nu}_\ell$ yield smaller uncertainties. Finally, we obtain the branching ratios $\mathcal{BR}(\bar{B}^0 \to \bar{K}^{*0}\nu_\ell\bar{\nu}_\ell) = 8.09(96) \times 10^{-6}$, $\mathcal{BR}(\bar{B}^+ \to \bar{K}^{*+}\nu_\ell\bar{\nu}_\ell) = 9.95(1.05) \times 10^{-6}$, and the longitudinal K^* polarization fraction $F_L = 0.44(4)$.

For the $b \to s$ induced flavor-changing neutral current processes, a crucial task is to improve the precision of the $B \to K^*$ form factors. It can be further improved with respect to the following three aspects: developing model-independent methods for accurately describing the B-meson light cone distribution amplitudes; reducing the uncertainties in the nonperturbative input parameters, such as the inverse moment λ_B of the leading-twist B-meson LCDA; extending calculations to next-to-next-to-leading order at leading power and NLO at subleading power, and imposing stricter unitarity bounds on the z-series parametrizations to further constrain uncertainties.

Ultimately, we emphasize that our improved $B \to K^*$ form factors are crucial for investigating flavor-changing neutral current processes and determining the branching ratios of the electroweak penguin processes $B \to K^*\nu_\ell\bar{\nu}_\ell$. With the high luminosity Belle II experimental data upcoming, our predictions will be further tested in the future.

ACKNOWLEDGMENTS

We thank Shan Cheng for valuable discussions. Y.-L. S. acknowledges support from the National Natural Science Foundation of China with Grant No. 12175218, and the Natural Science Foundation of Shandong Province under Grant No. ZR2024 MA076. D.-H. L. acknowledges support from the National Natural Science Foundation of China with Grant No. 12447154. The work of U. G. M. was supported in part by the CAS President's International Fellowship Initiative (PIFI) under Grant No. 2025PD0022.

DATA AVAILABILITY

The data that support the findings of this article are openly available [79].

APPENDIX A: HARD FUNCTION FOR THE SCET CURRENTS AT $\mathcal{O}(\alpha_s)$

Here we present the hard coefficient functions of A0-type and B1-type SCET_I currents in $B \to K^*$ form factors up to $\mathcal{O}(\alpha_s)$

$$C_{f_+}^{(\mathrm{A0})} = 1 + \frac{\alpha_s C_F}{4\pi}\left\{-2\ln^2\left(\frac{r}{\hat{\mu}}\right) + 5\ln\left(\frac{r}{\hat{\mu}}\right) - 2\mathrm{Li}_2(1-r) - 3\ln r - \frac{\pi^2}{12} - 6\right\}, \tag{A1}$$

$$C_{f_0}^{(\mathrm{A0})} = 1 + \frac{\alpha_s C_F}{4\pi}\left\{-2\ln^2\left(\frac{r}{\hat{\mu}}\right) + 5\ln\left(\frac{r}{\hat{\mu}}\right) - 2\mathrm{Li}_2(1-r) - \frac{3-5r}{1-r}\ln r - \frac{\pi^2}{12} - 4\right\}, \tag{A2}$$

$$C_{f_T}^{(\mathrm{A0})} = 1 + \frac{\alpha_s C_F}{4\pi}\left\{-2\ln\hat{\nu} - 2\ln^2\left(\frac{r}{\hat{\mu}}\right) + 5\ln\left(\frac{r}{\hat{\mu}}\right) - 2\mathrm{Li}_2(1-r) - \frac{3-r}{1-r}\ln r - \frac{\pi^2}{12} - 6\right\}, \tag{A3}$$

$$C_{V}^{(\mathrm{A0})} = 1 + \frac{\alpha_s C_F}{4\pi}\left\{-2\ln^2\left(\frac{r}{\hat{\mu}}\right) + 5\ln\left(\frac{r}{\hat{\mu}}\right) - 2\mathrm{Li}_2(1-r) - \frac{3-2r}{1-r}\ln r - \frac{\pi^2}{12} - 6\right\}, \tag{A4}$$

$$C_{T_1}^{(\mathrm{A0})} = 1 + \frac{\alpha_s C_F}{4\pi}\left\{-2\ln\hat{\nu} - 2\ln^2\left(\frac{r}{\hat{\mu}}\right) + 5\ln\left(\frac{r}{\hat{\mu}}\right) - 2\mathrm{Li}_2(1-r) - 3\ln r - \frac{\pi^2}{12} - 6\right\}, \tag{A5}$$

$$C_{f_+}^{(\mathrm{B1})} = (-2 + 1/r) + \mathcal{O}(\alpha_s), \qquad C_{f_0}^{(\mathrm{B1})} = (-1/r) + \mathcal{O}(\alpha_s), \tag{A6}$$

$$C_{f_T}^{(\mathrm{B1})} = (1/r) + \mathcal{O}(\alpha_s), \qquad C_{V}^{(\mathrm{B1})} = 0 + \mathcal{O}(\alpha_s), \qquad C_{T_1}^{(\mathrm{B1})} = -1 + \mathcal{O}(\alpha_s), \tag{A7}$$

where we introduced three variables

$$r = \frac{n\cdot p}{m_b}, \qquad \hat{\mu} = \frac{\mu}{m_b}, \qquad \hat{\nu} = \frac{\nu}{m_b}. \tag{A8}$$

APPENDIX B: EFFECTIVE B-MESON DISTRIBUTION AMPLITUDES

For brevity, we introduce the effective B-meson distribution amplitudes $\phi^-_{B,\mathrm{eff}}$, $\tilde{\phi}^-_{B,\mathrm{eff}}$ and $\phi^+_{B,m}$ absorbing the hard-collinear fluctuations,

$$\phi^-_{B,\mathrm{eff}}(\omega',\mu) = \phi^-_B(\omega',\mu) + \frac{\alpha_s C_F}{4\pi}\left\{\int_0^{\omega'} d\omega\left[\frac{2}{\omega-\omega'}\left(\ln\frac{\mu^2}{n\cdot p\omega'} - 2\ln\frac{\omega'-\omega}{\omega'}\right)\right]_\oplus \phi^-_B(\omega,\mu)\right.$$
$$\left. - \int_{\omega'}^{\infty} d\omega\left[\ln^2\frac{\mu^2}{n\cdot p\omega'} - \left(2\ln\frac{\mu^2}{n\cdot p\omega'} + 3\right)\ln\frac{\omega-\omega'}{\omega'} + 2\ln\frac{\omega}{\omega'} + \frac{\pi^2}{6} - 1\right]\frac{d\phi^-_B(\omega,\mu)}{d\omega}\right\}, \tag{B1}$$

$$\tilde{\phi}^-_{B,\mathrm{eff}}(\omega',\mu,\nu) = \phi^-_B(\omega',\mu) + \frac{\alpha_s C_F}{4\pi}\left\{\int_0^{\omega'} d\omega\left[\frac{2}{\omega-\omega'}\left(\ln\frac{\mu^2}{n\cdot p\omega'} - 2\ln\frac{\omega'-\omega}{\omega'} - \frac{1}{2}\right)\right]_\oplus \phi^-_B(\omega,\mu)\right.$$
$$\left. - \int_{\omega'}^{\infty} d\omega\left[\ln^2\frac{\mu^2}{n\cdot p\omega'} - \ln\frac{\nu^2}{n\cdot p\omega'} - \left(2\ln\frac{\mu^2}{n\cdot p\omega'} + 4\right)\ln\frac{\omega-\omega'}{\omega'} + 2\ln\frac{\omega}{\omega'} + \frac{\pi^2}{6} - 1\right]\frac{d\phi^-_B(\omega,\mu)}{d\omega}\right\}, \tag{B2}$$

$$\phi^+_{B,m}(\omega',\mu) = \frac{\alpha_s C_F}{4\pi} m_q \int_{\omega'}^{\infty} d\omega \ln\frac{\omega-\omega'}{\omega'}\frac{d}{d\omega}\frac{\phi^+_B(\omega,\mu)}{\omega}. \tag{B3}$$

The plus function that appeared in the above equations is defined by

$$\int_0^{\omega'} d\omega[f(\omega,\omega')]_\oplus g(\omega) = \int_0^{\omega'} d\omega f(\omega,\omega')[g(\omega) - g(\omega')]. \tag{B4}$$

APPENDIX C: DISPERSION INTEGRAL FORMULAS

After Borel transformation, the dispersion functions appearing in the factorization formulas of the $B \to K^*$ form factors are listed in the following:

$$f_{2,1}[\phi(\omega)] = -\int_0^{\omega_s} d\omega e^{-\frac{\omega}{\omega_M}}\phi(\omega),$$
$$f_{2,2}[\phi(\omega)] = e^{-\frac{\omega_s}{\omega_M}}\phi(\omega_s) + \int_0^{\omega_s} d\omega\frac{e^{-\frac{\omega}{\omega_M}}}{\omega_M}\phi(\omega),$$
$$f_{3,2}[\phi(\omega_1,\omega_2,u)] = e^{-\frac{\omega_s}{\omega_M}}\int_0^{\omega_s} d\omega_1\int_{\omega_s-\omega_1}^{\infty}\frac{d\omega_2}{\omega_2}\phi\left(\omega_1,\omega_2,\frac{\omega_s-\omega_1}{\omega_2}\right)$$
$$+ \int_0^{\omega_s} d\omega\int_0^{\omega} d\omega_1\int_{\omega-\omega_1}^{\infty}\frac{d\omega_2}{\omega_2}\frac{e^{-\frac{\omega}{\omega_M}}}{\omega_M}\phi\left(\omega_1,\omega_2,\frac{\omega-\omega_1}{\omega_2}\right),$$
$$f_{3,3}[\phi(\omega_1,\omega_2,u)] = -\frac{1}{2}e^{\frac{-\omega_s}{\omega_M}}\left\{\int_{\omega_s}^{\infty}\frac{d\omega_2}{\omega_2}\phi\left(0,\omega_2,\frac{\omega_s}{\omega_2}\right)\right.$$
$$\left. + \int_0^{\omega_s} d\omega_1\int_{\omega_s-\omega_1}^{\infty}\frac{d\omega_2}{\omega_2}\left(\frac{d}{d\omega_1} + \frac{1}{\omega_M}\right)\phi\left(\omega_1,\omega_2,\frac{\omega_s-\omega_1}{\omega_2}\right)\right\}$$
$$- \frac{1}{2\omega_M^2}\int_0^{\omega_s} d\omega\int_0^{\omega} d\omega_1\int_{\omega-\omega_1}^{\infty}\frac{d\omega_2}{\omega_2}e^{\frac{-\omega}{\omega_M}}\phi\left(\omega_1,\omega_2,\frac{\omega-\omega_1}{\omega_2}\right), \tag{C1}$$

where ϕ stands for the general B-meson LCDAs or their combinations appearing in the function $f_{i,j}$. The function $f_{i,j}$ describes the contribution of terms in the form $\phi(\omega)/(\omega-\cdots)^j$, with $\phi(\omega)$ being the i-particle LCDA and the denominator raised to the j-th power.

APPENDIX D: MODELING THE B-MESON LCDAS

The general ansatz for leading- and higher-twist B-meson LCDAs at the reference scale $\mu_0 = 1$ GeV [54] can be systematically established in such a way that both tree-level equations of motion constraints and the normalization conditions of the LCDAs [45,50] are satisfied:

$$
\begin{aligned}
\phi_B^+(\omega) &= \omega\mathbb{F}(\omega;-1), \qquad \phi_B^{-\mathrm{WW}}(\omega) = \mathbb{F}(\omega;0),\\
\phi_B^{-\mathrm{t3}}(\omega) &= \frac{1}{6}\mathcal{N}(\lambda_E^2-\lambda_H^2)[-\omega^2\mathbb{F}(\omega;-2)+4\omega\mathbb{F}(\omega;-1)-2\mathbb{F}(\omega;0)],\\
\phi_3(\omega_1,\omega_2) &= \frac{1}{2}\mathcal{N}(\lambda_E^2-\lambda_H^2)\omega_1\omega_2^2\mathbb{F}(\omega_1+\omega_2;-2),\\
\hat{g}_B^+(\omega) &= \frac{1}{4}[2\omega(\omega-\bar{\Lambda})\mathbb{F}(\omega;0)+(3\omega-2\bar{\Lambda})\mathbb{F}(\omega;1)+3\mathbb{F}(\omega;2)-\frac{1}{6}\mathcal{N}(\lambda_E^2-\lambda_H^2)\omega^2\mathbb{F}(\omega;0)],\\
\hat{g}_B^-(\omega) &= \frac{1}{4}\{(3\omega-2\bar{\Lambda})\mathbb{F}(\omega;1)+3\mathbb{F}(\omega;2)\\
&\quad+\frac{1}{3}\mathcal{N}(\lambda_E^2-\lambda_H^2)\omega[\omega(\bar{\Lambda}-\omega)\mathbb{F}(\omega;-1)-\left(2\bar{\Lambda}-\frac{3}{2}\omega\right)\mathbb{F}(\omega;0)]\},\\
\phi_4(\omega_1,\omega_2) &= \frac{1}{2}\mathcal{N}(\lambda_E^2+\lambda_H^2)\omega_2^2\mathbb{F}(\omega_1+\omega_2;-1),\\
\psi_4(\omega_1,\omega_2) &= \mathcal{N}\lambda_E^2\omega_1\omega_2\mathbb{F}(\omega_1+\omega_2;-1), \qquad \tilde{\psi}_4(\omega_1,\omega_2) = \mathcal{N}\lambda_H^2\omega_1\omega_2\mathbb{F}(\omega_1+\omega_2;-1),\\
\phi_5(\omega_1,\omega_2) &= \mathcal{N}(\lambda_E^2+\lambda_H^2)\omega_1\mathbb{F}(\omega_1+\omega_2;0), \qquad \psi_5(\omega_1,\omega_2) = -\mathcal{N}\lambda_E^2\omega_2\mathbb{F}(\omega_1+\omega_2;0),\\
\tilde{\psi}_5(\omega_1,\omega_2) &= -\mathcal{N}\lambda_H^2\omega_2\mathbb{F}(\omega_1+\omega_2;0),\\
\phi_6(\omega_1,\omega_2) &= \mathcal{N}(\lambda_E^2-\lambda_H^2)\mathbb{F}(\omega_1+\omega_2;1),
\end{aligned}
\tag{D1}
$$

where

$$
\begin{aligned}
\mathcal{N} &= \frac{1}{3}\frac{\beta(\beta+1)}{\alpha(\alpha+1)}\frac{1}{\omega_0^2}, \qquad \bar{\Lambda} = \frac{3}{2}\frac{\alpha}{\beta}\omega_0,\\
\mathbb{F}(\omega;n) &\equiv \omega_0^{n-1}U(\beta-\alpha,2-n-\alpha,\omega/\omega_0)\frac{\Gamma(\beta)}{\Gamma(\alpha)}e^{-\omega/\omega_0},
\end{aligned}
\tag{D2}
$$

with $U(a,b,z)$ as the hypergeometric U function. The appearing HQET parameters λ_E^2 and λ_H^2 at the reference scale $\mu_0 = 1$ GeV are defined by the matrix element of the local quark-gluon-quark operator,

$$
\langle 0|\bar{q}(0)g_sG_{\mu\nu}(0)\Gamma h_v(0)|\bar{B}(v)\rangle = -\frac{i}{6}\tilde{f}_B(\mu)m_B\lambda_H^2\mathrm{Tr}[\gamma_5\Gamma P_+\sigma_{\mu\nu}]-\frac{1}{6}\tilde{f}_B(\mu)m_B(\lambda_H^2-\lambda_E^2)\mathrm{Tr}[\gamma_5\Gamma P_+(v_\mu\gamma_\nu-v_\nu\gamma_\mu)]. \tag{D3}
$$

The matrix element can be estimated adopting QCD sum rules yielding

$$
\lambda_E^2 = 0.11 \pm 0.06\ \mathrm{GeV}^2, \qquad \lambda_H^2 = 0.18 \pm 0.07\ \mathrm{GeV}^2, \qquad [45] \tag{D4}
$$

$$
\lambda_E^2 = 0.03 \pm 0.02\ \mathrm{GeV}^2, \qquad \lambda_H^2 = 0.06 \pm 0.03\ \mathrm{GeV}^2, \qquad [91] \tag{D5}
$$

$$
\lambda_E^2 = 0.01 \pm 0.01\ \mathrm{GeV}^2, \qquad \lambda_H^2 = 0.15 \pm 0.05\ \mathrm{GeV}^2, \qquad [92] \tag{D6}
$$

where we take into account that the method used to estimate λ_E^2 and λ_H^2, as discussed in Ref. [91], unfortunately not only disrupts the convergence of the operator-product-expansion, but also enhances the contributions from the continuum and higher excited states. Therefore, we will use the numerical results of λ_E^2 and λ_H^2 from Table I, which can cover the ranges allowed by Refs. [45,92], and simultaneously satisfy the upper bounds imposed by Ref. [91].

We expect that the model for B-meson light cone distribution amplitudes is only valid in the small momenta region and the inverse logarithmic moments are only sensitive to the small momentum behavior of the distribution amplitude. Employing the definitions of inverse logarithmic moments of the leading-twist B-meson LCDA,

$$\frac{1}{\lambda_B(\mu)} = \int_0^\infty \frac{d\omega}{\omega}\phi_B^+(\omega,\mu),$$
$$\frac{\hat{\sigma}_n(\mu)}{\lambda_B(\mu)} = \int_0^\infty \frac{d\omega}{\omega}\ln^n\frac{e^{-\gamma_E}\lambda_B(\mu)}{\omega}\phi_B^+(\omega,\mu), \quad \text{(D7)}$$

we can determine the parameters of the three-parameter model for B-meson light cone distribution amplitudes in Eq. (D1),

$$\lambda_B(\mu) = \frac{\alpha-1}{\beta-1}\omega_0,$$
$$\hat{\sigma}_1(\mu) = \psi(\beta-1) - \psi(\alpha-1) + \ln\frac{\alpha-1}{\beta-1},$$
$$\hat{\sigma}_2(\mu) = \hat{\sigma}_1^2(\mu) + \psi'(\alpha-1) - \psi'(\beta-1) + \frac{\pi^2}{6}, \quad \text{(D8)}$$

where γ_E and $\psi(x)$ denote the Euler-Mascheroni constant and the digamma function, respectively. The scale dependence of these moments at the one-loop level is given by

$$\frac{\lambda_B(\mu_0)}{\lambda_B(\mu)} = 1 + \frac{\alpha_s(\mu_0)C_F}{4\pi}\ln\frac{\mu}{\mu_0}\left[2 - 2\ln\frac{\mu}{\mu_0} - 4\sigma_1(\mu_0)\right],$$
$$\hat{\sigma}_1(\mu) = \hat{\sigma}_1(\mu_0) + \frac{\alpha_s(\mu_0)C_F}{4\pi}4\ln\frac{\mu}{\mu_0}[\hat{\sigma}_1^2(\mu_0) - \hat{\sigma}_2(\mu_0)]. \quad \text{(D9)}$$

Then we construct the LL resummation (evolution) for the twist-two and three two-particle B-meson LCDAs. The explicit expressions can be found in Ref. [54]:

$$\phi_B^+(\omega,\mu) = U_\phi(\mu,\mu_0)\frac{1}{\omega^{p+1}}\frac{\Gamma(\beta)}{\Gamma(\alpha)}\mathcal{G}(\omega;0,2,1),$$
$$\phi_B^{-\mathrm{WW}}(\omega,\mu) = U_\phi(\mu,\mu_0)\frac{1}{\omega^{p+1}}\frac{\Gamma(\beta)}{\Gamma(\alpha)}\mathcal{G}(\omega;0,1,1),$$
$$\phi_B^{-\mathrm{t3}}(\omega,\mu) = -\frac{1}{6}U_\phi^{\mathrm{t3}}(\mu,\mu_0)\mathcal{N}(\lambda_E^2-\lambda_H^2)\frac{\omega_0^2}{\omega^{p+3}}\frac{\Gamma(\beta)}{\Gamma(\alpha)}\left\{\mathcal{G}(\omega;0,3,3)\right.$$
$$\left. + (\beta-\alpha)\left[\frac{\omega}{\omega_0}\mathcal{G}(\omega;0,2,2) - \beta\frac{\omega}{\omega_0}\mathcal{G}(\omega;1,2,2) - \mathcal{G}(\omega;1,3,3)\right]\right\}, \quad \text{(D10)}$$

where $p = \frac{\Gamma_{\mathrm{cusp}}^{(0)}}{2\beta_0}\ln[\alpha_s(\mu)/\alpha_s(\mu_0)]$, the twist-three two-particle LCDA $\phi_B^-(\omega,\mu) = \phi_B^{-WW}(\omega,\mu) + \phi_B^{-\mathrm{t3}}(\omega,\mu)$ is a linear combination of the (twist-two) Wandzura-Wilczek (WW) term and the genuine twist-three term, and

$$\mathcal{G}(\omega;l,m,n) \equiv G_{23}^{21}\left(\frac{\omega}{\omega_0}\middle|{}^{1,\beta+l}_{p+m,\alpha,p+n}\right) \quad \text{(D11)}$$

denotes the Meijer $\mathcal{G}$ function. The evolution factors $U_\phi(\mu,\mu_0)$ and $U_\phi^{\mathrm{t3}}(\mu,\mu_0)$ are given explicitly at one-loop order [50,93],

$$U_\phi(\mu,\mu_0) = \exp\left\{-\frac{\Gamma_{\mathrm{cusp}}^{(0)}}{4\beta_0^2}\left(\frac{4\pi}{\alpha_s(\mu_0)}\left[\ln r - 1 + \frac{1}{r}\right] - \frac{\beta_1}{2\beta_0}\ln^2 r + \left(\frac{\Gamma_{\mathrm{cusp}}^{(1)}}{\Gamma_{\mathrm{cusp}}^{(0)}} - \frac{\beta_1}{\beta_0}\right)[r - 1 - \ln r]\right)\right\}(e^{2\gamma_E}\mu_0)^{\frac{\Gamma_{\mathrm{cusp}}^{(0)}}{2\beta_0}\ln r}\, r^{\frac{\gamma_{\mathrm{t2}}^{(0)}}{2\beta_0}},$$
$$U_\phi^{\mathrm{t3}}(\mu,\mu_0) = U_\phi(\mu,\mu_0)|_{\gamma_{\mathrm{t2}}^{(0)}\to\gamma_{\mathrm{t2}}^{(0)}+\gamma_{\mathrm{t3}}^{(0)}}, \quad \text{(D12)}$$

where $r = \alpha_s(\mu)/\alpha_s(\mu_0)$, $\Gamma_{\mathrm{cusp}}^{(i)}$ are the cusp anomalous dimensions at various orders and

$$\gamma_{\mathrm{t2}}^{(0)} = -2C_F, \qquad \gamma_{\mathrm{t3}}^{(0)} = 2N_c. \quad \text{(D13)}$$

Both evolution factors satisfy the boundary condition at the reference scale μ_0:

$$U_\phi(\mu_0,\mu_0) = 1, \qquad U_\phi^{\mathrm{t3}}(\mu_0,\mu_0) = 1. \quad \text{(D14)}$$

[1] M. Algueró, A. Biswas, B. Capdevila, S. Descotes-Genon, J. Matias, and M. Novoa-Brunet, Eur. Phys. J. C **83**, 648 (2023).
[2] R. Aaij *et al.* (LHCb Collaboration), Phys. Rev. Lett. **125**, 011802 (2020).
[3] B. Capdevila, A. Crivellin, and J. Matias, Eur. Phys. J. Spec. Top. **1**, 20 (2023).
[4] I. Adachi *et al.* (Belle-II Collaboration), Phys. Rev. D **109**, 112006 (2024).
[5] M. Beneke, T. Feldmann, and D. Seidel, Nucl. Phys. **B612**, 25 (2001).
[6] M. Beneke, T. Feldmann, and D. Seidel, Eur. Phys. J. C **41**, 173 (2005).
[7] J. Lyon and R. Zwicky, Phys. Rev. D **88**, 094004 (2013).
[8] A. Khodjamirian, T. Mannel, A. A. Pivovarov, and Y. M. Wang, J. High Energy Phys. 09 (2010) 089.
[9] N. Gubernari, D. van Dyk, and J. Virto, J. High Energy Phys. 02 (2021) 088.
[10] A. J. Buras, J. Girrbach-Noe, C. Niehoff, and D. M. Straub, J. High Energy Phys. 02 (2015) 184.
[11] B. Allanach and A. Mullin, J. High Energy Phys. 09 (2023) 173.
[12] B. F. Hou, X. Q. Li, M. Shen, Y. D. Yang, and X. B. Yuan, J. High Energy Phys. 06 (**2024**) 172.
[13] R. R. Horgan, Z. Liu, S. Meinel, and M. Wingate, Phys. Rev. D **89**, 094501 (2014).
[14] R. R. Horgan, Z. Liu, S. Meinel, and M. Wingate, Proc. Sci. LATTICE2014 (**2015**) 372 [arXiv:1501.00367].
[15] M. Beneke and T. Feldmann, Nucl. Phys. **B592**, 3 (2001).
[16] C. W. Bauer, D. Pirjol, and I. W. Stewart, Phys. Rev. D **67**, 071502 (2003).
[17] M. Beneke and T. Feldmann, Nucl. Phys. **B685**, 249 (2004).
[18] M. Beneke, A. P. Chapovsky, M. Diehl, and T. Feldmann, Nucl. Phys. **B643**, 431 (2002).
[19] B. O. Lange and M. Neubert, Nucl. Phys. **B690**, 249 (2004); **B723**, 201(E) (2005).
[20] R. J. Hill, T. Becher, S. J. Lee, and M. Neubert, J. High Energy Phys. 07 (2004) 081.
[21] M. Beneke and D. Yang, Nucl. Phys. **B736**, 34 (2006).
[22] C. W. Bauer, S. Fleming, D. Pirjol, and I. W. Stewart, Phys. Rev. D **63**, 114020 (2001).
[23] M. Beneke, Y. Kiyo, and D. s. Yang, Nucl. Phys. **B692**, 232 (2004).
[24] P. Ball and V. M. Braun, Phys. Rev. D **55**, 5561 (1997).
[25] P. Ball and V. M. Braun, Phys. Rev. D **58**, 094016 (1998).
[26] P. Ball and R. Zwicky, Phys. Rev. D **71**, 014029 (2005).
[27] A. Bharucha, D. M. Straub, and R. Zwicky, J. High Energy Phys. 08 (2016) 098.
[28] A. Khodjamirian, T. Mannel, and N. Offen, Phys. Rev. D **75**, 054013 (2007).
[29] N. Gubernari, A. Kokulu, and D. van Dyk, J. High Energy Phys. 01 (2019) 150.
[30] F. De Fazio, T. Feldmann, and T. Hurth, J. High Energy Phys. 02 (2008) 031.
[31] J. Gao, C. D. Lü, Y. L. Shen, Y. M. Wang, and Y. B. Wei, Phys. Rev. D **101**, 074035 (2020).
[32] A. Khodjamirian, B. Melić, and Y. M. Wang, Eur. Phys. J. Spec. Top. **233**, 271 (2024).
[33] S. Cheng, A. Khodjamirian, and J. Virto, Phys. Rev. D **96**, 051901 (2017).
[34] S. Descotes-Genon, A. Khodjamirian, and J. Virto, J. High Energy Phys. 12 (2019) 083.
[35] S. Descotes-Genon, A. Khodjamirian, J. Virto, and K. K. Vos, J. High Energy Phys. 06 (2023) 034.
[36] B. Y. Cui, Y. K. Huang, Y. L. Shen, C. Wang, and Y. M. Wang, J. High Energy Phys. 03 (2023) 140.
[37] J. Gao, T. Huber, Y. Ji, C. Wang, Y. M. Wang, and Y. B. Wei, J. High Energy Phys. 05 (2022) 024.
[38] B. Y. Cui, Y. K. Huang, Y. M. Wang, and X. C. Zhao, Phys. Rev. D **108**, L071504 (2023).
[39] S. Okubo, Phys. Rev. D **4**, 725 (1971).
[40] C. Bourrely, B. Machet, and E. de Rafael, Nucl. Phys. **B189**, 157 (1981).
[41] C. Bourrely, I. Caprini, and L. Lellouch, Phys. Rev. D **79**, 013008 (2009); **82**, 099902(E) (2010).
[42] F. De Fazio, T. Feldmann, and T. Hurth, Nucl. Phys. **B733**, 1 (2006); **B800**, 405(E) (2008).
[43] Y. M. Wang and Y. L. Shen, Nucl. Phys. **B898**, 563 (2015).
[44] C. D. Lü, Y. L. Shen, Y. M. Wang, and Y. B. Wei, J. High Energy Phys. 01 (2019) 024.
[45] A. G. Grozin and M. Neubert, Phys. Rev. D **55**, 272 (1997).
[46] M. Beneke and J. Rohrwild, Eur. Phys. J. C **71**, 1818 (2011).
[47] M. Beneke and T. Feldmann, Phys. Lett. B **553**, 267 (2003).
[48] P. Colangelo and A. Khodjamirian, arXiv:hep-ph/0010175.
[49] A. K. Leibovich, Z. Ligeti, and M. B. Wise, Phys. Lett. B **564**, 231 (2003).
[50] V. M. Braun, Y. Ji, and A. N. Manashov, J. High Energy Phys. 05 (2017) 022.
[51] I. I. Balitsky and V. M. Braun, Nucl. Phys. **B311**, 541 (1989).
[52] M. Neubert, Phys. Rep. **245**, 259 (1994).
[53] A. F. Falk, M. Neubert, and M. E. Luke, Nucl. Phys. **B388**, 363 (1992).
[54] M. Beneke, V. M. Braun, Y. Ji, and Y. B. Wei, J. High Energy Phys. 07 (2018) 154.
[55] S. S. Agaev, V. M. Braun, N. Offen, and F. A. Porkert, Phys. Rev. D **83**, 054020 (2011).
[56] X. Y. Han *et al.* (Lattice Parton Collaboration), Phys. Rev. D **111**, 034503 (2025).
[57] S. Navas *et al.* (Particle Data Group), Phys. Rev. D **110**, 030001 (2024).
[58] Y. L. Shen, Y. M. Wang, and Y. B. Wei, J. High Energy Phys. 12 (2020) 169.
[59] M. Beneke, C. Bobeth, and Y. M. Wang, J. High Energy Phys. 12 (2020) 148.
[60] K. G. Chetyrkin, J. H. Kuhn, and M. Steinhauser, Comput. Phys. Commun. **133**, 43 (2000).
[61] Y. Aoki *et al.* (Flavour Lattice Averaging Group (FLAG)), Eur. Phys. J. C **82**, 869 (2022).
[62] C. Allton *et al.* (RBC-UKQCD Collaboration), Phys. Rev. D **78**, 114509 (2008).
[63] T. Janowski, B. Pullin, and R. Zwicky, J. High Energy Phys. 12 (2021) 008.
[64] P. Ball and E. Kou, J. High Energy Phys. 04 (2003) 029.
[65] R. Mandal, S. Nandi, and I. Ray, Phys. Lett. B **848**, 138345 (2024).
[66] S. J. Lee and M. Neubert, Phys. Rev. D **72**, 094028 (2005).
[67] T. Feldmann, B. O. Lange, and Y. M. Wang, Phys. Rev. D **89**, 114001 (2014).

[68] V. M. Braun, D. Y. Ivanov, and G. P. Korchemsky, Phys. Rev. D **69**, 034014 (2004).
[69] W. Wang, Y. M. Wang, J. Xu, and S. Zhao, Phys. Rev. D **102**, 011502 (2020).
[70] X. Y. Han, J. Hua, X. Ji, C. D. Lü, W. Wang, J. Xu, Q. A. Zhang, and S. Zhao, arXiv:2403.17492.
[71] P. Ball, V. M. Braun, Y. Koike, and K. Tanaka, Nucl. Phys. **B529**, 323 (1998).
[72] J. Brod, M. Gorbahn, and E. Stamou, Phys. Rev. D **83**, 034030 (2011).
[73] M. Bona *et al.* (UTfit Collaboration), Rend. Lincei Sci. Fis. Nat. **34**, 37 (2023).
[74] B. L. Ioffe, Phys. At. Nucl. **66**, 30 (2003).
[75] P. Gelhausen, A. Khodjamirian, A. A. Pivovarov, and D. Rosenthal, Phys. Rev. D **88**, 014015 (2013); **89**, 099901(E) (2014); **91**, 099901(E) (2015).
[76] Y. M. Wang and Y. L. Shen, J. High Energy Phys. 05 (2018) 184.
[77] L. Lellouch, Nucl. Phys. **B479**, 353 (1996).
[78] C. Bourrely and I. Caprini, Nucl. Phys. **B722**, 149 (2005).
[79] See Supplemental Material at http://link.aps.org/supplemental/10.1103/yvjd-2ymn for our combined fit results of the $B \to K^*$ form factors.
[80] E. Kou *et al.* (Belle-II Collaboration), Prog. Theor. Exp. Phys. **2019**, 123C01 (2019); **2020**, 029201(E) (2020).
[81] S. Halder (Belle-II Collaboration), arXiv:2101.11573.
[82] J. P. Lees *et al.* (*BABAR* Collaboration), Phys. Rev. D **87**, 112005 (2013).
[83] O. Lutz *et al.* (Belle Collaboration), Phys. Rev. D **87**, 111103 (2013).
[84] J. Grygier *et al.* (Belle Collaboration), Phys. Rev. D **96**, 091101 (2017).
[85] W. Altmannshofer, A. J. Buras, D. M. Straub, and M. Wick, J. High Energy Phys. 04 (2009) 022.
[86] T. Inami and C. S. Lim, Prog. Theor. Phys. **65**, 297 (1981); **65**, 1772(E) (1981).
[87] G. Buchalla and A. J. Buras, Nucl. Phys. **B398**, 285 (1993).
[88] G. Buchalla and A. J. Buras, Nucl. Phys. **B548**, 309 (1999).
[89] M. Misiak and J. Urban, Phys. Lett. B **451**, 161 (1999).
[90] J. F. Kamenik and C. Smith, Phys. Lett. B **680**, 471 (2009).
[91] M. Rahimi and M. Wald, Phys. Rev. D **104**, 016027 (2021).
[92] T. Nishikawa and K. Tanaka, Nucl. Phys. **B879**, 110 (2014).
[93] V. M. Braun, A. N. Manashov, and N. Offen, Phys. Rev. D **92**, 074044 (2015).